increased capillary density and organized capillary network in the engineered myocardial tissues, enhanced GFP-labeled EPCs originating from the transplanted cell sheet seemed to differentiate into an inner vWF- and vascular endothelial-cadherin–positive endothelial layer surrounded by an outer circumferential SMA-positive layer, partially derived from transplanted SMCs. The direct contribution of SMCs was confirmed by fluorescence in situ hybridization analysis of the myocardium, demonstrating new vasculature containing male SMCs in a female heart. Furthermore, the morphology of the vessel formation within myocardial tissues, including the diameter, composition, and stability of vessel walls, suggested that vessel maturation may occur under pathological stimuli. Furthermore, our data showed that coculturing EPCs with SMCs enhanced the secretion of TGFβ, which is thought to promote stabilization in multiple ways: the synthesis and deposition of ECM and contextual regulation of proliferation and differentiation.[17] Therefore, it is likely that the process of vessel maturation is a transition from an actively growing vessel to a quiescent fully functional mature vessel network via endothelial–pericyte interaction.

The mechanism by which the transplanted cocultured bi-level cell sheet attenuated ventricular remodeling and improved cardiac function, as shown in this study, seemed to depend on the cell sheet being placed over the scarred area of the myocardium and led to repair of the anterior wall thickness, reduction of LV wall stress, and the improvement of LV function. Previous studies indicated that the surviving myocardium and transplanted cell sheet attenuate complex cellular and molecular events, including hypertrophy, fibrosis, apoptosis of the myocardium, and the pathological accumulation of ECM.[7,23]

Cell engraftment is another critical aspect of myocardial regeneration. The potential advantages of the cell-sheet technology include the ability to deliver a larger number of transplanted cells that integrate with native tissues without destroying the cell–cell or cell–ECM adhesions in the cell-sheet.[7] Together with our significant findings of increased cell survival, integrin β1 upregulation, and the enhanced secretion of HGF in vitro in the cell-sheet group, it is likely that the cocultured bi-level cell-sheet prolonged cell survival by preventing anoikis mediated by the ECM receptors, in particular via integrin β1, or modulated by growth factor (eg, HGF).[24]

This treatment strategy for acute myocardial infarction is not yet directly applicable to the clinical arena because of the time required to isolate, cultivate, and manipulate cells in vitro However, the finding that this therapy yielded marked cardioprotective effects through angiogenesis should be beneficial for treating other types of cardiac pathologies, such as the chronic phase of myocardial infarction.

A potential limitation of this study is that the optimal number of transplanted cells was unknown in vivo. In addition, further studies are necessary to determine the optimal mixing ratio of transplanted EPCs and SMCs. We believe that this scaffold-free cell-sheet technique seems to be more transplantable to humans.[15] Although the cocultured bi-level cell sheet maintained different cell types in separate layers in vitro, our in vivo findings showed that the transplanted cell sheet could be a mixture of both cell types. This is probably because each cell type possessed different cell affinity, cell–matrix attachment, and migration ability.

In conclusion, we found that coculturing EPCs with SMCs in a bi-level cell-sheet delivery system enhanced the angiogenic effect by facilitating more architecturally mature microvascular formation. We also observed that bi-level cell-sheet technology initiated robust angiogenesis and regulated vessel maturation, thereby reducing fibrosis, attenuating ventricular remodeling, and improving cardiac function in ischemic cardiomyopathic rats. These findings suggest that novel bi-level cell-sheet technology creates an avenue of powerful cardiac repair. This concept may lead to new regeneration therapies in advanced cardiomyopathy.

Acknowledgments

We thank Dr Arudo Hiraoka, Dr Masaki Taira, and Akima Harada for their excellent technical assistances. We also thank Dr Takashi Daimon, Department of Biostatistics, Hyogo College of Medicine, for his statistical assessment.

Sources of Funding

This study was supported by the National Institutes of Health grant 1R01HL089315 (to Dr Woo), the American Heart Association Great Rivers Affiliate Postdoctoral Fellowship cosponsored by the Claude R. Joyner Fund for Young Medical Researchers (No. 12POST12060567; to Dr Shudo), and the Shinya Fund for International Exchange, Japan (Dr Shudo).

Disclosures

None.

References

1. Hiesinger W, Perez-Aguilar JM, Atluri P, Marotta NA, Frederick JR, Fitzpatrick JR 3rd, McCormick RC, Muenzer JR, Yang EC, Levit RD, Yuan LJ, Macarthur JW, Saven JG, Woo YJ. Computational protein design to reengineer stromal cell-derived factor-1α generates an effective and translatable angiogenic polypeptide analog. *Circulation.* 2011;124(11 suppl):S18–S26.
2. Frederick JR, Fitzpatrick JR 3rd, McCormick RC, Harris DA, Kim AY, Muenzer JR, Marotta N, Smith MJ, Cohen JE, Hiesinger W, Atluri P, Woo YJ. Stromal cell-derived factor-1alpha activation of tissue-engineered endothelial progenitor cell matrix enhances ventricular function after myocardial infarction by inducing neovasculogenesis. *Circulation.* 2010;122(11 suppl):S107–S117.
3. Atluri P, Panlilio CM, Liao GP, Hiesinger W, Harris DA, McCormick RC, Cohen JE, Jin T, Feng W, Levit RD, Dong N, Woo YJ. Acute myocardial rescue with endogenous endothelial progenitor cell therapy. *Heart Lung Circ.* 2010;19:644–654.
4. Hagège AA, Marolleau JP, Vilquin JT, Alhéritière A, Peyrard S, Duboc D, Abergel E, Messas E, Mousseaux E, Schwartz K, Desnos M, Menasché P. Skeletal myoblast transplantation in ischemic heart failure: long-term follow-up of the first phase I cohort of patients. *Circulation.* 2006;114(1 suppl):I108–I113.
5. Schächinger V, Erbs S, Elsässer A, Haberbosch W, Hambrecht R, Hölschermann H, Yu J, Corti R, Mathey DG, Hamm CW, Süselbeck T, Assmus B, Tonn T, Dimmeler S, Zeiher AM; REPAIR-AMI Investigators. Intracoronary bone marrow-derived progenitor cells in acute myocardial infarction. *N Engl J Med.* 2006;355:1210–1221.
6. Assmus B, Honold J, Schächinger V, Britten MB, Fischer-Rasokat U, Lehmann R, Teupe C, Pistorius K, Martin H, Abolmaali ND, Tonn T, Dimmeler S, Zeiher AM. Transcoronary transplantation of progenitor cells after myocardial infarction. *N Engl J Med.* 2006;355:1222–1232.
7. Miyagawa S, Roth M, Saito A, Sawa Y, Kostin S. Tissue-engineered cardiac constructs for cardiac repair. *Ann Thorac Surg.* 2011;91:320–329.
8. Imanishi Y, Miyagawa S, Maeda N, Fukushima S, Kitagawa-Sakakida S, Daimon T, Hirata A, Shimizu T, Okano T, Shimomura I, Sawa Y. Induced adipocyte cell-sheet ameliorates cardiac dysfunction in a mouse

myocardial infarction model: a novel drug delivery system for heart failure. *Circulation*. 2011;124(11 suppl):S10–S17.
9. Shudo Y, Miyagawa S, Fukushima S, Saito A, Shimizu T, Okano T, Sawa Y. Novel regenerative therapy using cell-sheet covered with omentum flap delivers a huge number of cells in a porcine myocardial infarction model. *J Thorac Cardiovasc Surg*. 2011;142:1188–1196.
10. Sekine H, Shimizu T, Hobo K, Sekiya S, Yang J, Yamato M, Kurosawa H, Kobayashi E, Okano T. Endothelial cell coculture within tissue-engineered cardiomyocyte sheets enhances neovascularization and improves cardiac function of ischemic hearts. *Circulation*. 2008;118(14 suppl):S145–S152.
11. Kobayashi H, Shimizu T, Yamato M, Tono K, Masuda H, Asahara T, Kasanuki H, Okano T. Fibroblast sheets co-cultured with endothelial progenitor cells improve cardiac function of infarcted hearts. *J Artif Organs*. 2008;11:141–147.
12. Dzau VJ, Braun-Dullaeus RC, Sedding DG. Vascular proliferation and atherosclerosis: new perspectives and therapeutic strategies. *Nat Med*. 2002;8:1249–1256.
13. Atluri P, Liao GP, Panlilio CM, Hsu VM, Leskowitz MJ, Morine KJ, Cohen JE, Berry MF, Suarez EE, Murphy DA, Lee WM, Gardner TJ, Sweeney HL, Woo YJ. Neovasculogenic therapy to augment perfusion and preserve viability in ischemic cardiomyopathy. *Ann Thorac Surg*. 2006;81:1728–1736.
14. Asahara T, Murohara T, Sullivan A, Silver M, van der Zee R, Li T, Witzenbichler B, Schatteman G, Isner JM. Isolation of putative progenitor endothelial cells for angiogenesis. *Science*. 1997;275:964–967.
15. Sawa Y, Miyagawa S, Sakaguchi T, Fujita T, Matsuyama A, Saito A, Shimizu T, Okano T. Tissue engineered myoblast sheets improved cardiac function sufficiently to discontinue LVAS in a patient with DCM: report of a case. *Surg Today*. 2012;42:181–184.
16. Urbich C, Aicher A, Heeschen C, Dernbach E, Hofmann WK, Zeiher AM, Dimmeler S. Soluble factors released by endothelial progenitor cells promote migration of endothelial cells and cardiac resident progenitor cells. *J Mol Cell Cardiol*. 2005;39:733–742.
17. Li M, Nishimura H, Iwakura A, Wecker A, Eaton E, Asahara T, Losordo DW. Endothelial progenitor cells are rapidly recruited to myocardium and mediate protective effect of ischemic preconditioning via "imported" nitric oxide synthase activity. *Circulation*. 2005;111:1114–1120.
18. Rehman J, Li J, Orschell CM, March KL. Peripheral blood "endothelial progenitor cells" are derived from monocyte/macrophages and secrete angiogenic growth factors. *Circulation*. 2003;107:1164–1169.
19. Coussens LM, Werb Z. Inflammation and cancer. *Nature*. 2002;420:860–867.
20. Madonna R, Rokosh G, De Caterina R, Bolli R. Hepatocyte growth factor/Met gene transfer in cardiac stem cells–potential for cardiac repair. *Basic Res Cardiol*. 2010;105:443–452.
21. Risau W. Mechanisms of angiogenesis. *Nature*. 1997;386:671–674.
22. Goumans MJ, Valdimarsdottir G, Itoh S, Rosendahl A, Sideras P, ten Dijke P. Balancing the activation state of the endothelium via two distinct TGF-beta type I receptors. *EMBO J*. 2002;21:1743–1753.
23. Golocheikine A, Tiriveedhi V, Angaswamy N, Benshoff N, Sabarinathan R, Mohanakumar T. Cooperative signaling for angiogenesis and neovascularization by VEGF and HGF following islet transplantation. *Transplantation*. 2010;90:725–731.
24. Zvibel I, Smets F, Soriano H. Anoikis: roadblock to cell transplantation? *Cell Transplant*. 2002;11:621–630.

EUROPEAN SOCIETY OF CARDIOLOGY®

Cardiovascular Research (2013) **99**, 102–110
doi:10.1093/cvr/cvt088

Transplantation of myoblast sheets that secrete the novel peptide SVVYGLR improves cardiac function in failing hearts

Ayako Uchinaka[1], Naomasa Kawaguchi[1,2]*, Yoshinosuke Hamada[1], Seiji Mori[1], Shigeru Miyagawa[3], Atsuhiro Saito[4], Yoshiki Sawa[3], and Nariaki Matsuura[1]

[1]Department of Molecular Pathology, Osaka University Graduate School of Medicine, Suita, Japan; [2]Department of Cardiovascular Pathology, Division of Health Sciences, Osaka University Graduate School of Medicine, Suita, Japan; [3]Department of Cardiovascular Surgery, Osaka University Graduate School of Medicine, Suita, Japan; and [4]Medical Center of Translational Research, Osaka University Hospital, Osaka University Graduate School of Medicine, Suita, Japan

Received 4 December 2012; revised 27 March 2013; accepted 7 April 2013; online publish-ahead-of-print 23 April 2013

Time for primary review: 52 days

Aims Transplantation of myoblast sheets is a promising therapy for enhancing cardiac function after heart failure. We have previously demonstrated that a 7-amino-acid sequence (Ser-Val-Val-Tyr-Gly-Leu-Arg) derived from osteopontin (SV peptide) induces angiogenesis. In this study, we evaluated the long-term therapeutic effects of myoblast sheets secreting SV in a rat infarction model.

Methods and results Two weeks after ligation of the left anterior descending coronary artery, the animals were divided into the following three groups: a group transplanted with wild-type rat skeletal myoblast sheets (WT-rSkMs); a group transplanted with SV-secreting myoblast sheets (SV-rSkMs); and a control group (ligation only). We evaluated cardiac function, histological changes, and smooth muscle actin (SMA) expression through transforming growth factor-β (TGF-β) signalling. The ejection fraction and fractional shortening were significantly better, and the enlargement of end-systolic volume was also significantly attenuated in the SV-rSkM group. Left ventricular remodelling, including fibrosis and hypertrophy, was significantly attenuated in the SV-rSkM group, and SV secreted by the myoblast sheets promoted angiogenesis in the infarcted border area. Furthermore, many clusters of SMA-positive cells were observed in the infarcted areas in the SV-rSkM group. *In vitro* SMA expression was increased when SV was added to the isolated myocardial fibroblasts. Moreover, SV bound to the TGF-β receptor, and SV treatment activated TGF-β receptor–Smad signalling.

Conclusion The SV-secreting myoblast sheets facilitate a long-term improvement in cardiac function. The SV can induce differentiation of fibroblasts to myofibroblasts via TGF-β–Smad signalling. This peptide could possibly be used as a bridge to heart transplantation or as an ideal peptide drug for cardiac regeneration therapy.

Keywords Cell therapy • Peptides • Myocardial infarction • Myofibroblats • Transforming growth factor-β

1. Introduction

In heart failure, tissue damage processes caused by ischaemia, such as cell death, fibrosis, and hypertrophy, gradually progress until the cardiac tissue becomes dysfunctional.[1–3] Transplantation of myoblast sheets is a promising treatment for ischaemic heart failure, and can inhibit left ventricular (LV) remodelling and improve cardiac function via paracrine effectors.[4–8] The cell-sheet technique avoids the arrhythmogenicity associated with skeletal myoblast therapy by injection.[9]

However, this treatment has failed to achieve long-term therapeutic effects, because the transplanted sheets are exposed to blood and nutrient deprivation and drop out from the injured myocardium. Recent studies demonstrated that myoblast sheets that overexpress different cardioprotective agents display enhanced therapeutic effects.[10,11] Therefore, the combined application of gene therapy with angiogenic agents and myoblast sheet transplantation may achieve sustained therapeutic efficacy. Through the secretion of angiogenic factors from transplanted myoblasts, the newly formed blood vessels can supply blood flow to the surviving myocardium and the transplanted

* Corresponding author: 1-7 Yamada-oka, Suita, Osaka 565-0871, Japan. Tel: +81 6 6879 2588; fax: +81 6 6879 2588, E-mail: kawaguch@sahs.med.osaka-u.ac.jp

cells, and the functional deterioration of ischaemic cardiomyopathy should thus improve in the long term.

Osteopontin is a multifunctional cytokine expressed during healing and fibrotic processes.[12] We have previously reported that the osteopontin-derived peptide Ser-Val-Val-Tyr-Gly-Leu-Arg (SVVYGLR; SV) exhibits angiogenic activity *in vitro* and *in vivo*,[13–17] and that its angiogenic activity is as potent as that of vascular endothelial growth factor (VEGF).[14] Owing to their high molecular weights, the most well-known angiogenesis-promoting factors, namely, VEGF and hepatocyte growth factor (HGF), are resistant to degradation. In contrast, peptides such as SV are more easily degraded by peptidase within an organism and show only a few adverse effects, such as oedema and pleural fluid accumulation.[18–20] This indicates the high biocompatibility of peptides.

In this study, we hypothesized that the augmentation of myoblast sheets by SV gene transfer could improve cardiac function in the long term.

2. Methods

2.1 Animal ethics

Animal care complied with the 'Guide for Care and Use of Laboratory Animals' (NIH publication no. 85-23, revised 1996). The Ethics Review Committee for Animal Experimentation of Osaka University Graduate School of Medicine approved the experimental protocols.

2.2 Isolation of skeletal myoblasts and sheets

After induction of general anaesthesia with pentobarbital (300 mg/kg) and heparin (150 U) by intraperitoneal injection, myoblasts were isolated from the skeletal muscle of the tibialis anterior muscle of 3-week-old male Lewis rats. The muscles were minced and enzymatically dissociated with 0.2% collagenase type II (Worthington Biochemical Corp., Lakewood, NJ, USA) and trypsin at 37°C. The isolated cells were suspended in Dulbecco's modified Eagle's medium with 20% fetal bovine serum. After being pre-plated twice, non-adherent cells were then plated on a dish coated with Matrigel (Becton Dickinson Bioscience, Franklin Lakes, NJ, USA) and incubated at 37°C in humidified air enriched with 5% CO_2. We maintained the cell densities at <70% confluence to prevent skeletal myoblast differentiation that would result in myotube formation. Myoblast sheets were formed by plating 3×10^6 infected myoblasts on a temperature-responsive culture dish (UpCell; CellSeed, Tokyo, Japan).

2.3 Animal model and myoblast sheet transplantation

The myocardial infarction (MI) models were generated via ligation of the left anterior descending (LAD) coronary artery in 8-week-old female F344/NJcl-rnu/rnu rats. The rats were anaesthetized by inhalation of isoflurane (2%, 0.2 mL/min), intubated, and placed on a respirator during surgery to maintain ventilation. The carrier gas for isoflurane is oxygen. The adequacy of anaesthesia was monitored by electrocardiography and pulse rate. Two weeks after ligation of the LAD coronary artery, the myoblast sheets were transplanted. The rats were randomly divided into the following three groups: (i) a WT-rat skeletal myoblast (rSkM) group (transplanted with three wild-type myoblast sheets, $n = 6$); (ii) an SV-rSkM group (transplanted with three SV-secreting myoblast sheets, $n = 8$); and (iii) a control group (sham operation, $n = 6$). Each sheet was individually applied to the infarcted area.

2.4 Overexpression and transfection of SV

A lentiviral vector containing the complementary DNA (cDNA) of SV (SV/pCS-CG) was constructed (*Figure 1A*). The cDNA of SV was synthesized using DNA oligonucleotides. The primer sequences were as follows: forward, 1,5′-GCGCCACCATGGAGACAGACACACTCCTGCTATGGGTACTGCTGCTCTGGGTTCCAGGT-3′; forward, 2,5′-TCCACTGGTGACGCGGCCCAGCCGGCCAGTGTGGTTTATGGACTGAGGCTCGAGTACCCATACGATGTTCCAGATTACGCTTAAC-3′; reverse, 1,5′-TCGAGTTAAGCGTAATCTGGAACATCGTATGGGTACTCGAGCCTCAGTCCATAAACCACACT-3′; and reverse, 2,5′-GGCCGGCTGGGCCGCGTCACCAGTGGAACCTGGAACCCAGAGCAGCAGTACCCATAGCAGGAGTGTGTCTGTCTCCATGGTGGCG-3′.

The synthesized DNA oligonucleotides were linked and ligated to pCS-CG, and the isolated rSkMs were infected via incubation for 48 h in the presence of SV/pCS-CG.

2.5 Dot blotting assay

The culture media were used for the assays. Each sample was coated onto a black 96-well microplate overnight. To evaluate the secretion SV volume, the serially diluted solution of SV-HA peptide was also coated onto the plate as a control. After blocking, the primary antibody against the HA tag (Santa Cruz Biotechnology, Santa Cruz, CA, USA) was added to each well. After washing, anti-rabbit IgG-linked horseradish peroxidase (GE Healthcare, Piscataway, NJ, USA) was added. After washing, the plate was exposed to an Enhanced Chemiluminescence (ECL) kit (GE Healthcare).

2.6 Measurement of cardiac function

The cardiac function of the treated rats was evaluated by echocardiography 2, 4, 6, and 8 weeks after sheet transplantation. Baseline measurements were

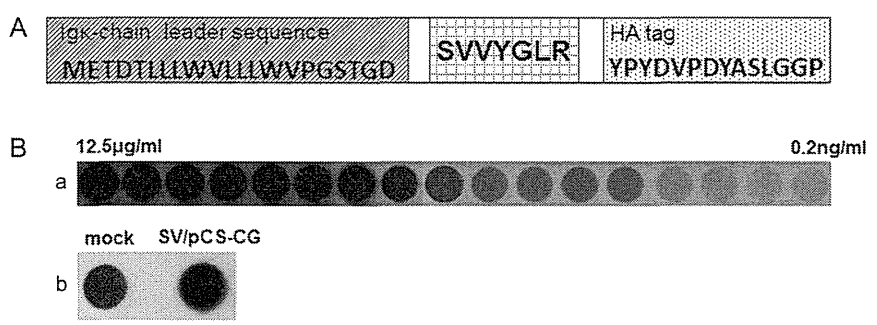

Figure 1 Assessment of SV expression. (*A*) View showing the frame format of the constructed SV gene. (*B*) Expression of SV in rSkMs infected with SV/pCS-CG by dot blotting: (*a*) the dilution series of SV-HA peptide; and (*b*) control cells infected with the empty vector (mock, left) and rSkMs infected with SV/pCS-CG (right).

made before sheet transplantation. The measurements were made using a SONOS 5500 sonograph (Philips Electronics, Tokyo, Japan) with a 12 MHz transducer under general anaesthesia induced and maintained by inhalation of isoflurane (2%, 0.2 mL/min) as mentioned above. The LV end-systolic area, LV end-diastolic area, and LV dimensions at end diastole and end systole (LVIDd and LVIDs, respectively) were determined. The ejection fraction (EF), fractional shortening (FS), end-diastolic volume (EDV), and end-systolic volume (ESV) were calculated as follows:

$$\text{LVEF}\ (\%) = (\text{LVDd}^3 - \text{LVDs}^3)/\text{LVDd}^3 \times 100\ (\%)$$
$$\text{LV\%FS} = [(\text{LVDd} - \text{LVDs})/\text{LVDd}] \times 100\ (\%)$$
$$\text{EDV} = \text{LVIDd}^3 \times (0.98 \times \text{LVIDd} + 5.90)\ (\text{mL})$$
$$\text{ESV} = \text{LVIDs}^3 \times (1.14 \times \text{LVIDs} + 4.18)\ (\text{mL})$$

2.7 Heart weight/body weight ratio

The body weights (BW; in grams) of the rats were measured 8 weeks after sheet transplantation, after which the rats were anaesthetized with pentobarbital (300 mg/kg) and heparin (150 U) by intraperitoneal injection, and their hearts were rapidly removed and weighed (in milligrams). The heart weight (HW)/BW ratio was then calculated.

2.8 Histological analyses

Myocardial specimens were obtained 8 weeks post-transplantation. The formalin-fixed samples were embedded in paraffin. The LV chamber diameter and the anterior wall thickness were measured from sections stained with haematoxylin and eosin. Infarcted wall thickness, posterior wall thickness, and LV chamber diameter were measured with the scale loupe. The sections were evaluated morphologically using the NIS Elements system (Nikon, Tokyo, Japan). Sirius Red staining was used to detect fibrosis. The percentage of fibrosis was calculated from the fibrotic ratio in the infarct border area. Periodic acid–Schiff staining for cardiomyocyte hypertrophy was also performed. We randomly selected 100 cardiomyocytes and measured the two-point shortest axes at the level of the nucleus.

Immunohistochemical staining for von Willebrand factor antigen was used to label vascular endothelial cells to permit the counting of blood vessels. The sections were incubated with primary antibody against von Willebrand factor (rabbit polyclonal; Dako, Glostrup, Denmark). The sections were incubated with a biotinylated anti-rabbit IgG antibody (Dako) and further incubated with peroxidase-conjugated streptavidin (SA; GE Healthcare). Visualization was performed with biphenyl-3,3′,4,4′-tetramine solution (Sigma, St Louis, MO, USA). The stained vascular endothelial cells were counted under a light microscope.

The distribution of myofibroblast-like cells was evaluated by immunohistochemical staining with anti-smooth muscle actin (SMA) antibody (Dako) and anti-smooth muscle myosin heavy chain (SM-MHC) type 2 antibody (Abcam Ltd, Cambridge, UK). The SMA-positive cell density was calculated as SMA positive area/infarcted area × 100 (%).

2.9 Primary culture of adult ventricular fibroblasts

Cardiac fibroblasts (CFs) were isolated from 8-week-old adult male Sprague–Dawley rats 4 weeks after the induction of MI by LAD ligation. The hearts were excised from anaesthetized rats and quickly transferred to Hank's buffered salt solution. The minced left ventricular tissues were digested using 100 U/mL type II collagenase and 0.1% trypsin at 37°C. The cells were centrifuged and suspended in Dulbecco's modified Eagle's medium supplemented with 10% fetal bovine serum, and incubated at 37°C in humidified air enriched with 5% CO_2.

2.10 Immunofluorescence staining

The isolated fibroblasts were incubated with SV (10 μg/mL), SV random peptide (GYRVLSV; 10 μg/mL), or transforming growth factor-β1 (TGF-β1; 25 ng/mL) for 72 h. The cells were fixed with 4% paraformaldehyde and incubated with anti-SMA antibody followed by incubation with cyanine-3-conjugated anti-rabbit secondary antibody (GE Healthcare). The nuclei were stained with 4′,6-diamino-2-phenylindole (DAPI; Invitrogen Life Technologies, Grand Island, NY, USA), and the fluorescent signals were detected by fluorescence microscopy (ECLIPSE E600, Nikon).

2.11 Western blotting assay

The isolated fibroblasts were incubated with SV (10 μg/mL), SV random peptide (10 μg/mL), or TGF-β1 (25 ng/mL) for 72 h. The cells were suspended in lysis buffer (50 mM Tris at pH 8.0, 120 mM NaCl, 1 mM EDTA, and 0.5% Nonidet P-40). Proteins in whole-cell lysates were separated by SDS–PAGE, transferred to a polyvinylidene fluoride transfer membrane (Millipore, Billerica, MA, USA), and probed sequentially with antibodies against SMA and α-tubulin (Sigma). The blots were developed using an ECL kit.

To examine the activity of TGF-β receptor–Smad signalling induced by SV, the phosphorylation of Smad2, Smad3, and TGF-β receptor I (TβRI) was studied by western blotting. The isolated fibroblasts were incubated with SV (10 μg/mL), SV random peptide (10 μg/mL), or TGF-β1 (25 ng/mL) for 1 h. Primary antibodies against phospho-Smad2, phospho-Smad3, Smad2/3 (Cell Signaling Technology, Inc., Danvers, MA, USA), TβRI (phospho S165; Abcam), and α-tubulin were used.

2.12 Construction of recombinant transforming growth factor-β receptorII

A pcDNA3.1 vector containing the cDNA encoding TβRII (pcDNA3.1-TβRII) was constructed. The recombinant TβRII was produced by transfecting HEK 293T cells with pcDNA3.1-TβRII. The culture media containing recombinant TβRII were harvested. The purification of recombinant TβRII was done using immunoprecipitation with anti-TβRII antibody.

2.13 Biacore analysis

The binding of SV to TβRII was assessed by Biacore analysis. Biotinylated SVs were captured on SA-coated BIAcore SA sensor chips (GE Healthcare, Piscataway, NJ, USA). Ligands were diluted to 10 μg/mL and injected at 10 μL/mL. To correct for refractive index change, non-specific binding, and instrument drift, a reference flow cell contained the SA-coated surface only. The recombinant TβRII was diluted to 10 μg/mL in Hank's buffered salt solution and injected during the association phase for 5 min (30 μL/min).

2.14 *In situ* proximity ligation assay

The Duolink *in situ* proximity ligation assay (PLA; Olink Biosciences, Uppsala, Sweden) was performed according to the manufacturer's protocol. The isolated fibroblasts were incubated in the presence of SV-HA peptide or SV-HA random peptide (GYRVLSV; 1 μg/mL) for 1 h. The fixed fibroblasts were incubated with the following primary antibodies: rabbit polyclonal anti-TβRII (Abcam) and mouse monoclonal anti-HA (Nacalai Tesque). The cells were then incubated with PLA probes consisting of two secondary anti-rabbit and anti-mouse antibodies, each tagged with an oligonucleotide. A hybridization solution consisting of two oligonucleotide linkers complementary to each PLA probe was added to the cells. The isolated cells were incubated with a Duolink Ligation stock containing ligase and Duolink polymerase. In addition, the cells were incubated with a detection solution consisting of fluorescently labelled oligonucleotides that hybridize to the rolling circle amplification product. The PLA signal was visualized using fluorescence microscopy.

2.15 Statistical analyses

Data are presented as the means ± SEM. Cardiac function was analysed by repeated-measures analysis of variance (ANOVA) for differences across the entire time course, as well as one-way ANOVA, whereas the Tukey–Kramer *post hoc* test was used to examine significant differences at each time point. To assess the significance of the differences between individual groups for

other data, statistical comparisons were performed using Student's unpaired *t*-test. $P < 0.05$ was considered statistically significant.

3. Results

3.1 Overexpression of SV in rat skeletal myoblasts

The signal strength of dots in wells coated with the culture medium of SV/pCS-CG-infected rSkMs was stronger than that of dots in wells coated with the culture medium of mock-infected rSkMs (*Figure 1B[b]*). The SV was synthesized and secreted by SV/pCS-CG-infected rSkMs. In addition, from the dilution series of SV-HA peptide, the secretion volume of SV was calculated to be approximately 3.125–6.25 ng/mL (*Figure 1B[a]*).

3.2 Effect of SV-secreting myoblast sheet on left ventricular function

Echocardiography revealed significantly better values of LVEF and %FS in the WT-rSkM and SV-rSkM groups compared with the control group at all time points after transplantation ($P < 0.01$). Although there were still significant differences between the control and WT-rSkM groups after the 4 week time point, the LVEF and %FS in the WT-rSkM group decreased dramatically. Furthermore, LVEF and %FS were significantly better in the SV-rSkM group at 2, 6, and 8 weeks after transplantation compared with the WT-rSkM group (2 and 6 weeks, $P < 0.05$; 8 weeks, $P < 0.01$; *Figure 2A* and *B*).

The evaluation of LVIDs illustrated the inhibition of dilatation in the SV-rSkM group in comparison with the control and WT-rSkM groups. In particular, at 6 and 8 weeks after transplantation LVIDs was significantly attenuated in the SV-rSkM group compared with the control group (6 weeks $P < 0.05$; 8 weeks $P < 0.01$; *Table 1*). The enlargement of ESV was also significantly attenuated in the SV-rSkM group compared with the control group at 6 and 8 weeks after transplantation (6 weeks, $P < 0.05$; 8 weeks, $P < 0.01$; *Table 1*). The increase in EDV was significantly inhibited in the SV-rSkM group compared with the control group only at 8 weeks after transplantation ($P < 0.05$; *Table 1*).

3.3 Heart weight/body weight ratio

We used the HW/BW ratio as an indicator of cardiac hypertrophy. The HW/BW ratio was significantly greater in the SV-rSkM group at 8 weeks after transplantation compared with the control and WT-rSkM groups ($P < 0.01$; *Figure 2C*).

3.4 Effect of SV-secreting myoblast sheet on left ventricular remodelling

Haematoxylin and eosin staining demonstrated thinning of the infarcted wall in the control and WT-rSkM groups, whereas the thickness of the infarcted wall was maintained in the SV-rSkM group (*Figure 2D* and *Table 2*). Statistical analysis demonstrated that the LV chamber of the SV-rSkM group was significantly less dilated that those of the control and WT-rSkM groups ($P < 0.05$; *Table 2*) and that the infarcted wall in the SV-rSkM group was significantly thicker than that in the control

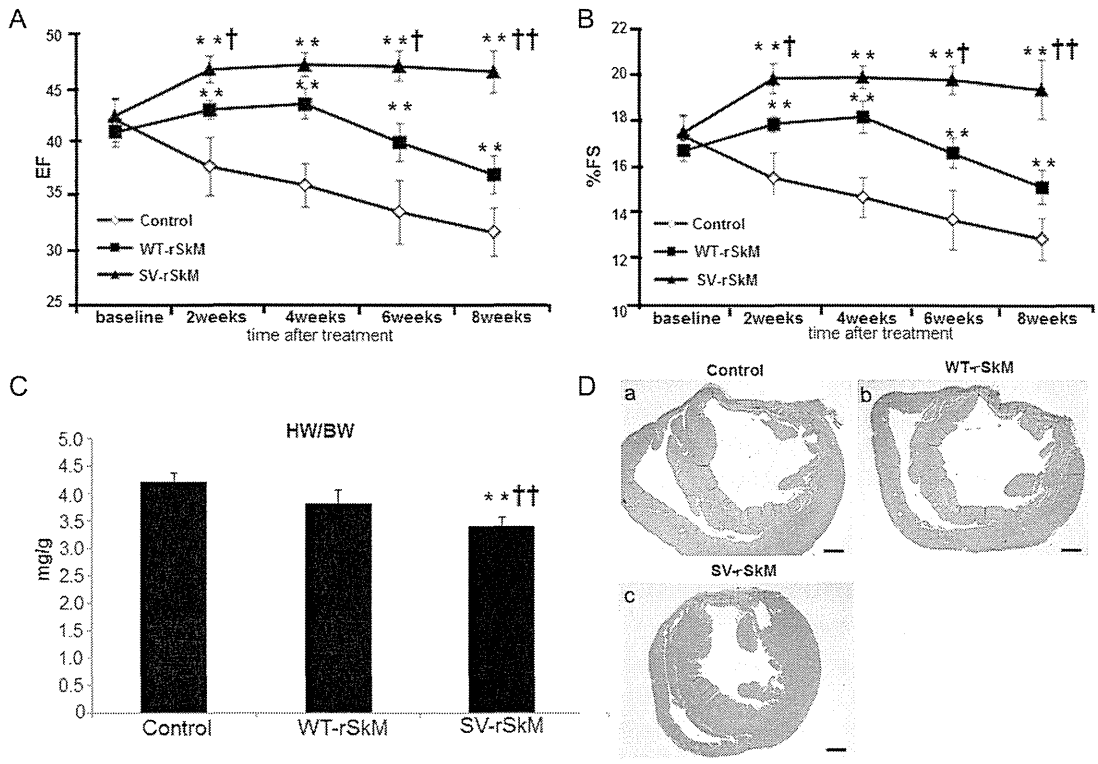

Figure 2 Echocardiographic evaluation of LV function after sheet transplantation (*A*, EF; *B*, %FS). $^{**}P < 0.01$ vs. Control group. $^{\dagger}P < 0.05$, $^{\dagger\dagger}P < 0.01$ vs. WT-rSkM group. Baseline is time of transplantation, which was 2 weeks after ligation of the LAD. Other times in weeks are post-transplantation. (*C*) Evaluation of HW/BW. $^{**}P < 0.01$ vs. Control group. $^{\dagger}P < 0.05$, $^{\dagger\dagger}P < 0.01$ vs. WT-rSkM group. (*D*) Haematoxylin- and eosin-stained section of the left ventricle: (*a*) control; (*b*) WT-rSkM; and (*c*) SV-rSkM (×10 magnification, scale bars represent 1000 μm).

Table 1 Assessment of LVIDd, LVIDs, EDV, and ESV over time by echocardiography

	Baseline	2 weeks	4 weeks	6 weeks	8 weeks
LVIDd (cm)					
Control	0.75 ± 0.04	0.77 ± 0.07	0.81 ± 0.05	0.87 ± 0.04	0.89 ± 0.01
WT-rSkM	0.76 ± 0.02	0.77 ± 0.04	0.80 ± 0.06	0.84 ± 0.06	0.85 ± 0.03
SV-rSkM	0.71 ± 0.05	0.78 ± 0.07	0.78 ± 0.07	0.83 ± 0.03	0.84 ± 0.03*
LVIDs (cm)					
Control	0.63 ± 0.02	0.67 ± 0.05	0.70 ± 0.05	0.75 ± 0.04	0.77 ± 0.02
WT-rSkM	0.63 ± 0.02	0.64 ± 0.03	0.67 ± 0.06	0.69 ± 0.05	0.72 ± 0.04
SV-rSkM	0.64 ± 0.04	0.65 ± 0.05	0.67 ± 0.04	0.67 ± 0.03*	0.69 ± 0.04**
EDV (ml)					
Control	2.87 ± 0.46	3.19 ± 0.93	3.65 ± 0.71	4.46 ± 0.63	4.79 ± 0.26
WT-rSkM	2.93 ± 0.24	3.04 ± 0.43	3.53 ± 0.77	4.05 ± 0.89	4.22 ± 0.54
SV-rSkM	2.77 ± 0.53	3.26 ± 0.70	3.37 ± 0.64	3.92 ± 0.43	4.08 ± 0.43*
ESV (ml)					
Control	1.20 ± 0.13	1.49 ± 0.36	1.71 ± 0.34	2.16 ± 0.40	2.34 ± 0.23
WT-rSkM	1.25 ± 0.14	1.28 ± 0.16	1.53 ± 0.37	1.69 ± 0.33	1.88 ± 0.22
SV-rSkM	1.29 ± 0.21	1.39 ± 0.27	1.48 ± 0.25	1.51 ± 0.23*	1.61 ± 0.25**

Abbreviations: EDV, end-diastolic volume; ESV; end-systolic volume; LVIDd, left ventricular dimensions at end diastole; LVIDs, left ventricular dimensions at end systole. Baseline is the time of transplantation, which was 2 weeks after ligation of the left anterior descending coronary artery; other times in weeks are post-transplantation. *$P < 0.05$, **$P < 0.01$ vs. control group at each time point.

and WT-rSkM groups ($P < 0.01$; *Table 2*). The values of the LV chamber diameter/posterior wall thickness were significantly lower in the SV-rSkM group compared with those in the control and WT-rSkM groups ($P < 0.01$; *Table 2*). There were no significant differences between the control and WT-rSkM groups regarding these indices.

The SV-rSkM group exhibited a significantly lower percentage of fibrosis than the control and WT-rSkM groups in the infarcted border area ($P < 0.01$; *Figure 3A*). The diameters of cardiomyocytes in the SV-rSkM group were significantly smaller than those in the control and WT-rSkM groups ($P < 0.01$; *Figure 3B*). There was no significant difference in the area remote from the transplant among the three groups.

3.5 The pro-angiogenic effects of SV

The capillary density 8 weeks after transplantation was significantly higher in the WT-rSkM and SV-rSkM groups than in the control group ($P < 0.01$). Furthermore, the capillary density in the SV-rSkM group was significantly higher than that in the WT-rSkM group ($P < 0.01$; *Figure 3C[a]–C[c]* and *D*). There was no significant difference in the area remote from the transplant among the three groups.

3.6 The accumulation of smooth muscle actin-positive and smooth muscle myosin heavy chain type2-positive cells by SV

Immunohistochemical staining with an anti-SMA antibody revealed that many clusters of SMA-positive cells were present in infarcted areas in the SV-rSkM group (*Figure 3E*). Statistical analysis indicated that the SMA-positive cell density was significantly higher in the WT-rSkM and SV-rSkM groups than in the control group (WT-rSkM , $P < 0.05$; SV-rSkM, $P < 0.01$; *Figure 3F*). Furthermore, the SMA-positive cell density was significantly higher in the SV-rSkM group than in the WT-rSkM group ($P < 0.05$; *Figure 3F*). Notably, SM-MHC type 2-positive cells were also detected in infarcted areas in the SV-rSkM group, whereas those cells were scarce in the control and WT-rSkM groups (*Figure 3G*).

Table 2 Thickness of the infarcted wall and posterior wall and left ventricular chamber diameter

	Control	WT-rSkM	SV-rSkM
Left ventricular chamber diameter (mm)	4.50 ± 0.46	4.48 ± 0.42	3.85 ± 0.29**††
Infarcted wall thickness (mm)	0.53 ± 0.05	0.51 ± 0.08	0.63 ± 0.06
Posterior wall thickness (mm)	2.04 ± 0.10	1.88 ± 0.25	1.96 ± 0.14
Percentage anterior wall thickness	25.98 ± 2.66	27.20 ± 2.63	32.29 ± 0.98**††
Left ventricular chamber diameter/ posterior wall thickness	2.36 ± 0.22	2.30 ± 0.15	1.98 ± 0.16**††

The percentage anterior wall thickness is the infarcted wall thickness/posterior wall thickness × 100. **$P < 0.01$ vs. control group. ††$P < 0.01$ vs. WT-rSkM group.

3.7 The induction of smooth muscle actin by SV

Expression of SMA was increased when SV was added to the isolated fibroblasts (*Figure 4A* and *B*). The expression level of SMA was similar to that of TGF-β1 (*Figure 4B*). Conversely, the expression level of SMA was unchanged by the addition of SV random peptide (*Figure 4A* and *B*).

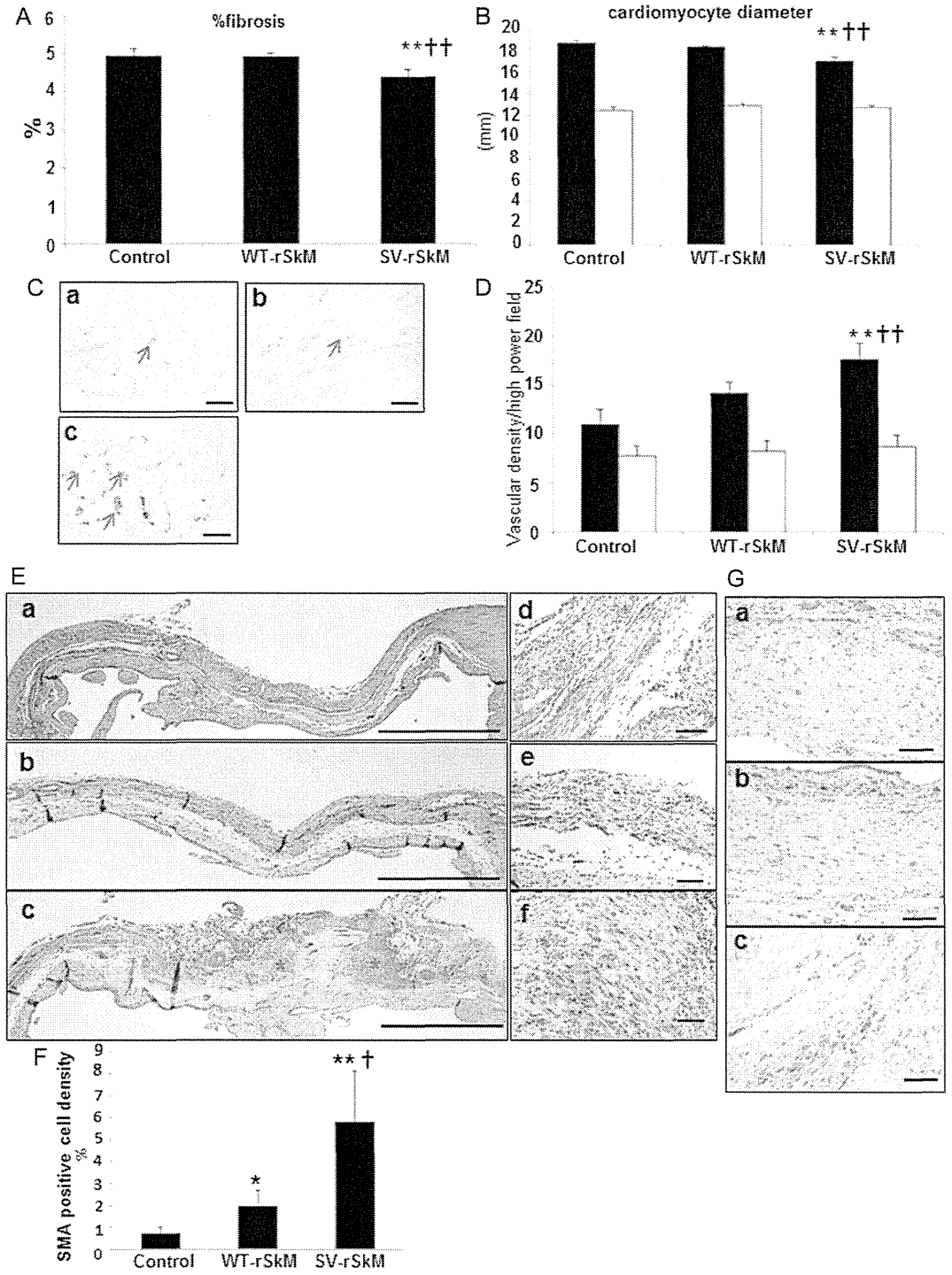

Figure 3 Histological evaluations of LV remodelling. (*A*) Percentage fibrosis. (*B*) Cardiomyocyte diameter. $^{**}P < 0.01$ vs. Control group. $^{\dagger\dagger}P < 0.01$ vs. WT-rSkM group. Filled bars, border area; open bars, remote area. Immunohistochemical staining. (*C*) A section of the infarcted border zone stained with an antibody against von Willebrand factor: (*a*) control; (*b*) WT-rSkM; and (*c*) SV-rSkM (×200 magnification, scale bars represent 100 μm). Newly formed vessel is stained brown. (*D*) Quantitative estimation of vascular density. $^{**}P < 0.01$ vs. Control group. $^{\dagger\dagger}P < 0.01$ vs. WT-rSkM group. Filled bars, border area; open bars, remote area. (*E*) The distribution of SMA-positive cells: (*a*) control; (*b*) WT-rSkM; (*c*) SV-rSkM (*a*–*c*, ×20 magnification, scale bars represent 1000 μm; e and *f*, ×200 magnification, scale bars represent 100 μm). Red asterisks denote SMA-positive cells. (*F*) Quantitative estimation of the SMA-positive cell density. $^{*}P < 0.05$, $^{**}P < 0.01$ vs. Control group. $^{\dagger}P < 0.05$ vs. WT-rSkM group. (*G*) The distribution of SM-MHC type 2-positive cells: (*a*) control; (*b*) WT-rSkM; and (*c*) SV-rSkM (*a*–*c*, ×200 magnification, scale bars represent 100 μm).

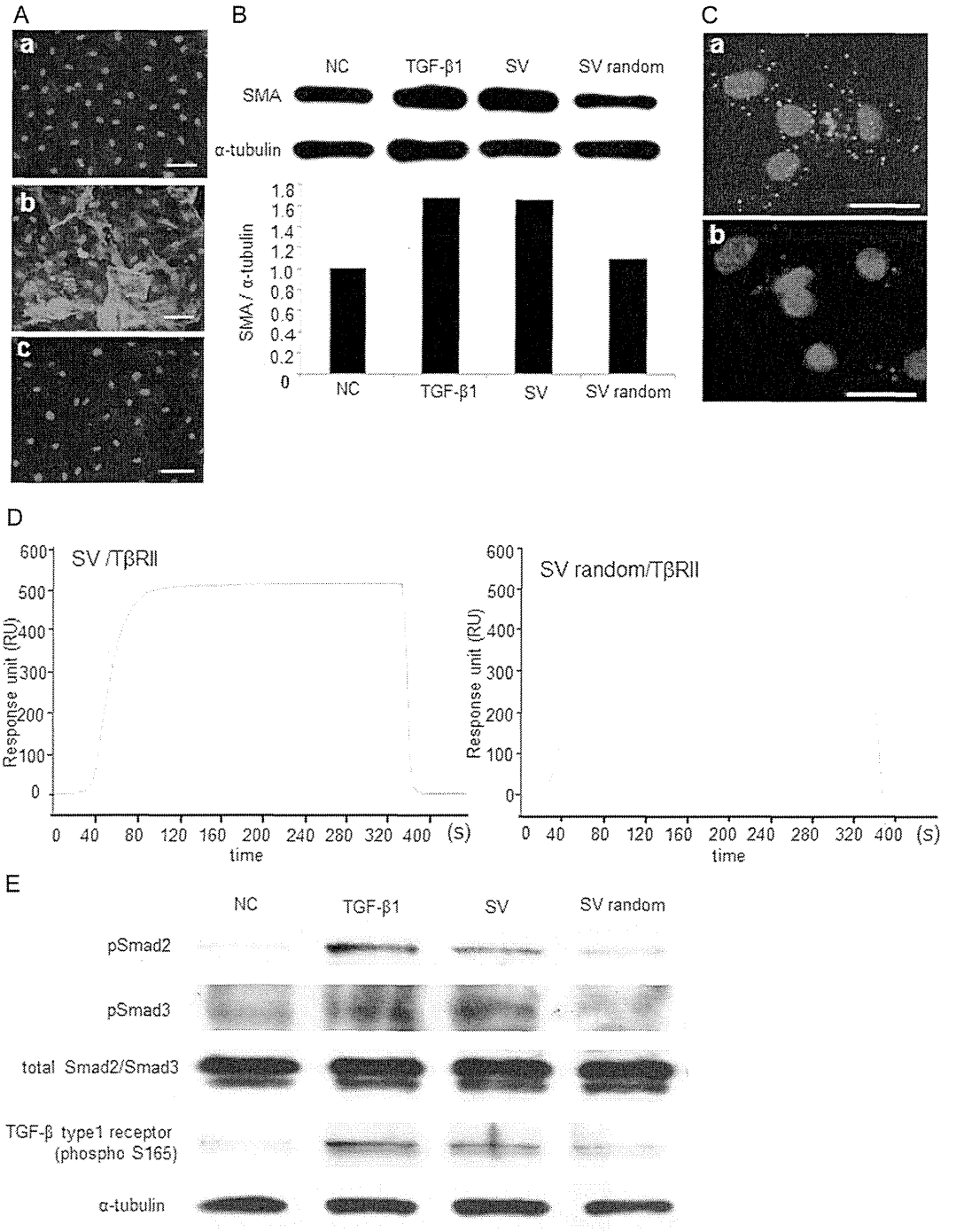

Figure 4 Myofibroblast differentiation induced by exposure of the isolated CFs to SV. (*A*) and (*B*) SMA expression induced by SV. (*A*) Immunofluorescence staining with an anti-SMA antibody: (*a*) non-stimulated CFs (NC); (*b*) CFs exposed to SV; and (*c*) CFs exposed to SV random peptide (×200 magnification, scale bars represent 100 μm). (*B*) Immunoblot of the myofibroblast differentiation marker SMA and its quantitative assessment. α-Tubulin was used as a loading control. (*C*) The examination of binding between TβRII and SV using an *in situ* PLA: (*a*) CFs exposed to SV; (*b*) CFs exposed to SV random peptide (scale bars represent 50 μm). The binding between TβRII and SV and the TGF-β–Smad signalling induced by SV. (*D*) Biacore analysis of the interaction of TβRII with SV. (*E*) Assessment of TGF-β–Smad signalling in CFs exposed to SV by western blotting. α-Tubulin was used as a loading control.

3.8 Binding of SV to transforming growth factor-β receptor II

When PLA was performed using rabbit polyclonal anti-TβRII and mouse monoclonal anti-HA antibodies for the isolated fibroblasts treated with SV-HA peptide, PLA-positive red signals were found (*Figure 4C[a]*). In contrast, PLA-positive red signals were not detected in the isolated fibroblasts treated with SV-HA random peptide (*Figure 4C[b]*). We assessed the ability of SV to bind to TβRII, using a sensor chip immobilized with biotinylated SV (K_D = 13.5 nM), and this peptide bound to TβRII with high affinity (500 Resonance Unit; *Figure 4D*). However, SV random peptides (K_D = 16 nM) had a much lower R_{max} (R_{max} = analyte molecular weight (MW)/ligand MW × the immobilization level × the stoichiometric ratio) value (200 Resonance Unit).

3.9 The effects of SV on Smad activation

Treatment with TGF-β1 or SV induced the phosphorylation of TβRI, Smad2, and Smad3 to similar degrees (*Figure 4E*). Conversely, treatment with SV random peptide had no effect on TβRI, Smad2, and Smad3 phosphorylation.

4. Discussion

In this study, we transplanted myoblast sheets to the myocardium in an infarcted rat model. The cell sheets are removed from special temperature-responsive dishes without destroying the cell–cell or cell–extracellular matrix adhesions in the cell sheet. The myoblast sheet does not require an artificial scaffold, because it has a great ability to integrate with the infarcted area via an adhesion factor, such as integrin-$\alpha_7\beta_1$ and α-dystroglycan, which are expressed on the surface of myoblasts; thus, the sheets do not fall off after the chest is closed.[5–7]

The effect of myoblast sheet transplantation is mediated mainly by paracrine growth factors that stimulate the injured myocardium.[6,7] The paracrine effectors include HGF, VEGF, and stromal-derived factor 1. These factors can promote angiogenesis in the ischaemic myocardium. Hepatocyte growth factor is also associated with anti-fibrosis and anti-apoptosis. The grafted myoblasts beneficially attract haematopoietic stem cells to home in on the infarcted heart area for heart regeneration and angiogenesis by stromal-derived factor 1.[6] These paracrine activities induce angiogenesis and reduce fibrosis and hypertrophy; as a result, the depressed cardiac function improves. Therefore, we hypothesized that functional modification of myoblast sheet properties by overexpressing a factor associated with angiogenesis, anti-fibrosis, and anti-apoptosis could further promote and maintain the therapeutic effects of the sheet. Our previous results demonstrated that SV has a much stronger pro-angiogenic action than VEGF.[14] Given that SV has a straight-chain sequence, rather than a complicated conformation, we can speculate that this peptide would be degraded by peptidase within an organism. Our previous research has shown that synthetic SV has no effect on the proliferation of endothelial and muscle cells.[13,14] The degradation rate and function for the proliferation of SV could have high biocompatibility with peptides. In this study, we investigated the effects of SV-secreting myoblast sheets in infarcted rat hearts.

Most of the transplanted myoblasts drop out at 4 weeks after sheet transplantation.[21] As a result, cardiac function in the WT-rSkM group at 4 weeks after sheet transplantation was markedly decreased. In contrast, in the SV-rSkM group the functional improvements were maintained for 8 weeks after sheet transplantation. The capillary density 8 weeks after transplantation was significantly higher in the SV-rSkM group than in the control and WT-rSkM groups. The vessels newly formed by the secreted SVs from the myoblast sheets remained until 8 weeks post-transplantation, after the drop-out of the transplanted cells. The paracrine factors from transplanted myoblasts also promoted angiogenesis. Thus, in this study, the secreted SV showed an enhanced angiogenic action after myoblast transplantation. It is possible that SV induced angiogenesis in both the surviving cardiomyocytes and the transplanted cells; as a result, the survival time of the transplanted cells would have been extended. However, there are no data concerning the effect of SV-rSkM on the endogenous mobilization/proliferation/apoptosis and differentiation of cardiac resident cardiac stem/progenitor cells. More research is needed to define the effects of SV on these cells.

Siltanen *et al.*[11] reported the efficacy of a heart failure treatment involving the transplantation of myoblasts genetically modified to overexpress HGF. Hepatocyte growth factor is a cardioprotective factor associated with angiogenesis, anti-fibrosis, and anti-apoptosis.[22,23] Hepatocyte growth factor-overexpressing myoblast sheets stimulated angiogenesis and inhibited myocardial fibrosis in a rat chronic heart failure model. However, cardiac function was not improved by the transplantation of HGF-overexpressing sheets.[16] In contrast, SV-expressing sheets, which also have a pro-angiogenic action, enhanced cardiac function and angiogenesis. Transplantation of SV-secreting sheets enhanced the functional recovery of ischaemic myocardium compared with the findings in the control and WT-rSkM groups. In particular, systolic parameters, such as LVIDs and ESV, were significantly improved in the SV-rSkM group.

Myofibroblasts share morphological features with fibroblasts and smooth muscle cells. Differentiated myofibroblasts are characterized by increased α-SMA and the morphological features of well-developed stress fibres.[24] Although myofibroblasts in normal tissue, granulation tissue, and pathological tissue exhibit phenotypic α-SMA expression, SM-MHC, vimentin, and desmin, myofibroblasts more commonly express α-SMA.[25] Myofibroblasts have a greater contractile capability than undifferentiated CFs, and this property is believed to be important in maintaining the structural integrity of healing scars.[26] Expression of α-SMA in stress fibres is instrumental in force generation by myofibroblasts.[27] Additionally, myofibroblasts confer mechanical tension to remodelling matrix via anchoring and contracting.[24] In this study, many clusters of SMA-positive and SM-MHC type 2-positive cells were observed in infarcted areas in the SV-rSkM group. These cells differentiated from CFs into myofibroblasts in the infarcted area after the addition of SV, and the myocardial contractile performance of the infarcted wall in the SV-rSkM group was improved by the accumulation of myofibroblasts. Our previous study indicated that, when skeletal myoblast sheets were transplanted into a swine acute MI model, well-developed smooth muscle cells accumulated in the centre of the scar.[28] In our study, more SMA-positive cells accumulated in the infarcted area in the SV-rSkM group than in the WT-rSkM-group, and the secreted SV enhanced the effect of SMA expression by CFs. Furthermore, owing to the accumulation of myofibroblasts in the infarcted area, adverse effects on the uninjured myocardium and its exercise endurance were decreased; consequently, cardiac remodelling processes, such as fibrosis and cardiomyocyte hypertrophy, were attenuated. The fibroblasts in scar tissue of the infarcted area are differentiated into SMA-positive and SM-MHC type 2-positive cells by SV. There is no cell–cell connectivity between these cells and the recipient's cardiomyocytes, and it is possible that they have not been synchronized with the cardiomyocytes. However, they do have a contractile capability, and SV could have transferred the contractility to the infarcted wall via the

accumulation of these cells, improving the motion of the scared left ventricular wall and inhibiting the dilatation of the LV chamber in the SV-rSkM group.

Our previous research has shown that synthetic SVVYGLR peptides *in vitro* activate the adhesion and migration of endothelial cells and smooth muscle cells, and stimulate tube formation by vascular endothelial cells.[13,14] In contrast, SV has no effect on the proliferation of these cells, whereas it enhances the adhesion and proliferation of several types of human mesenchymal cells.[17] Although the effects of SV on apoptosis in these cells have not been evaluated, the results regarding proliferation suggest that SV has no effect on apoptosis. According to these data, SV should have no impact on the proliferation and apoptosis of myoblasts, while stimulating the proliferation of fibroblasts and myofibroblasts.

Osteopontin is highly expressed during the differentiation of fibroblasts into myofibroblasts, and could have an effect on fibroblast differentiation and a role in myofibroblast function during tissue remodelling.[29] Transforming growth factor-β plays an important role in the activation of fibroblasts in wound repair, and it induces myofibroblast differentiation via Smad signalling.[30] Osteopontin is required for the differentiation and activation of myofibroblasts formed in response to TGF-β1.[31] This study illustrated that, in isolated CFs, SV had a great degree of affinity for TβRII and activated Smad signalling via TβRs. The secreted SV bound TβRII and induced the differentiation of fibroblasts into myofibroblasts through TGF-β receptor–Smad signalling.

Transforming growth factor-β participates in vascular development and the maintenance of vascular homeostasis, and it induces angiogenesis at low levels.[32] Transforming growth factor-β regulates angiogenesis by acting on both vascular endothelial and smooth muscle cells.[31] SV also stimulates angiogenesis at low levels, but this effect plateaus at high levels.[14] Thus, SV induces angiogenesis via the same mechanism as TGF-β. However, we believed that SV could also bind receptors other than TβRII and exhibit myocardium-protecting actions, such as promoting angiogenesis and inhibiting hypertrophy. To explain the effect of SV in improving cardiac function, SV receptors in myocardial tissue will have to be identified, and the details of its mechanism will need to be examined.

Functional SV peptide-secreting myoblast sheets facilitate long-term improvement in cardiac function and inhibition of cardiac remodelling. The SVs secreted from myoblast sheets effectively stimulated angiogenesis in the failing myocardium. The accumulation of SMA-positive cells induced by SV confers a contractile property on the infarcted wall. The early therapeutic effects after SV-secreting myoblast sheet transplantation were due to the paracrine effects of the transplanted myoblasts, and the late effects were caused by the pro-angiogenic effects of SV and its induction of myofibroblast accumulation via TGF-β–Smad signalling. These results suggest that SV could change CFs to muscle-like cells, allowing it to be used as a bridge to heart transplantation or as an ideal peptide drug for cardiac regeneration therapy.

Conflict of interest: none declared.

References

1. Buja LM, Vela D. Cardiomyocyte death and renewal in the normal and diseased heart. *Cardiovasc Pathol* 2008;**17**:349–374.
2. Gupta KB, Ratcliffe MB, Fallert MA, Edmunds LH Jr, Bogen DK. Changes in passive mechanical stiffness of myocardial tissue with aneurysm formation. *Circulation* 1994;**89**: 2315–2326.
3. Ciulla MM, Paliotti R, Ferrero S, Braidotti P, Esposito A, Gianelli U *et al.* Left ventricular remodeling after experimental myocardial cryoinjury in rats. *J Surg Res* 2004;**116**:91–97.
4. Okano T, Yamada N, Okuhara M, Sakai H, Sakurai Y. Mechanism of cell detachment from temperature-modulated, hydrophilic-hydrophobic polymer surfaces. *Biomaterials* 1995; **16**:297–303.
5. Kondoh H, Sawa Y, Miyagawa S, Sakakida-Kitagawa S, Memon IA, Kawaguchi N *et al.* Longer preservation of cardiac performance by sheet-shaped myoblast implantation in dilated cardiomyopathic hamsters. *Cardiovasc Res* 2006;**69**:466–475.
6. Memon IA, Sawa Y, Fukushima N, Matsumiya G, Miyagawa S, Taketani S *et al.* Repair of impaired myocardium by means of implantation of engineered autologous myoblast sheets. *J Thorac Cardiovasc Surg* 2005;**130**:1333–1341.
7. Miyagawa S, Sawa Y, Sakakida S, Taketani S, Kondoh H, Memon IA *et al.* Tissue cardiomyoplasty using bioengineered contractile cardiomyocyte sheets to repair damaged myocardium: their integration with recipient myocardium. *Transplantation* 2005;**80**: 1586–1595.
8. Memon IA, Sawa Y, Miyagawa S, Taketani S, Matsuda H. Combined autologous cellular cardiomyoplasty with skeletal myoblasts and bone marrow cells in canine hearts for ischemic cardiomyopathy. *J Thorac Cardiovasc Surg* 2005;**130**:646–653.
9. Narita T, Shintani Y, Ikebe C, Kaneko M, Harada N, Tshuma N *et al.* The use of cell-sheet technique eliminates arrhythmogenicity of skeletal myoblast-based therapy to the heart with enhanced therapeutic effects. *Int J Cardiol* 2012; pii: S0167-5273(12)01187-4. doi:10.1016/j.ijcard.2012.09.081. [Epub ahead of print].
10. Kitabayashi K, Siltanen A, Pätilä T, Mahar MA, Tikkanen I, Koponen J *et al.* Bcl-2 expression enhances myoblast sheet transplantation therapy for acute myocardial infarction. *Cell Transplant* 2010;**19**:573–588.
11. Siltanen A, Kitabayashi K, Lakkisto P, Mäkelä J, Pätilä T, Ono M *et al.* hHGF overexpression in myoblast sheets enhances their angiogenic potential in rat chronic heart failure. *PLoS One* 2011;**6**:e19161.
12. Sodek J, Ganss B, McKee MD. Osteopontin. *Crit Rev Oral Biol Med* 2000;**11**:279–303.
13. Hamada Y, Yuki K, Okazaki M, Fujitani W, Matsumoto T, Hashida MK *et al.* Osteopontin-derived peptide SVVYGLR induces angiogenesis *in vivo*. *Dent Mater J* 2004;**23**:650–655.
14. Hamada Y, Nokihara K, Okazaki M, Fujitani W, Matsumoto T, Matsuo M *et al.* Angiogenic activity of osteopontin-derived peptide SVVYGLR. *Biochem Biophys Res Commun* 2003; **310**:153–157.
15. Hamada Y, Egusa H, Kaneda Y, Hirata I, Kawaguchi N, Hirao T *et al.* Synthetic osteopontin-derived peptide SVVYGLR can induce neovascularization in artificial bone marrow scaffold biomaterials. *Dent Mater J* 2007;**26**:487–492.
16. Yokosaki Y, Matsuura N, Sasaki T, Murakami I, Schneider H, Higashiyama S *et al.* The integrin $\alpha_9\beta_1$ binds to a novel recognition sequence (SVVYGLR) in the thrombin-cleaved amino-terminal fragment of osteopontin. *J Biol Chem* 1999;**274**:36328–36334.
17. Egusa H, Kaneda Y, Akashi Y, Hamada Y, Matsumoto T, Saeki M *et al.* Enhanced bone regeneration via multimodal actions of synthetic peptide SVVYGLR on osteoprogenitors and osteoclasts. *Biomaterials* 2009;**30**:4676–4686.
18. Rissanen TT, Rutanen J, Ylä-Herttuala S. Gene transfer for therapeutic vascular growth in myocardial and peripheral ischemia. *Adv Genet* 2004;**52**:117–164.
19. Sack U, Hoffmann M, Zhao XJ, Chan KS, Hui DS, Gosse H *et al.* Vascular endothelial growth factor in pleural effusions of different origin. *Eur Respir J* 2005;**25**:600–604.
20. Kunig AM, Balasubramaniam V, Markham NE, Seedorf G, Gien J, Abman SH. Recombinant human VEGF treatment transiently increases lung edema but enhances lung structure after neonatal hyperoxia. *Am J Physiol Lung Cell Mol Physiol* 2006;**291**:L1068–L1078.
21. Saito S, Miyagawa S, Sakaguchi T, Imanishi Y, Iseoka H, Nishi H *et al.* Myoblast sheet can prevent the impairment of cardiac diastolic function and late remodeling after left ventricular restoration in ischemic cardiomyopathy. *Transplantation* 2012;**93**:1108–1115.
22. Nakamura Y, Morishita R, Higaki J, Kida I, Aoki M, Moriguchi A *et al.* Hepatocyte growth factor is a novel member of the endothelium-specific growth factors: additive stimulatory effect of hepatocyte growth factor with basic fibroblast growth factor but not with vascular endothelial growth factor. *J Hypertens* 1996;**14**:1067–1072.
23. Ono K, Matsumori A, Shioi T, Furukawa Y, Sasayama S. Enhanced expression of hepatocyte growth factor/c-Met by myocardial ischemia and reperfusion in a rat model. *Circulation* 1997;**95**:2552–2558.
24. Gabbiani G. The myofibroblast in wound healing and fibrocontractive diseases. *J Pathol* 2003;**200**:500–503.
25. Hinz B, Mastrangelo D, Iselin CE, Chaponnier C, Gabbiani G. Mechanical tension controls granulation tissue contractile activity and myofibroblast differentiation. *Am J Pathol* 2001;**159**:1009–1020.
26. Sun Y, Weber KT. RAS and connective tissue in the heart. *Int J Biochem Cell Biol* 2003;**35**: 919–931.
27. Hinz B, Celetta G, Tomasek JJ, Gabbiani G, Chaponnier C. Alpha-smooth muscle actin expression upregulates fibroblast contractile activity. *Mol Biol Cell* 2001;**12**:2730–2741.
28. Miyagawa S, Saito A, Sakaguchi T, Yoshikawa Y, Yamauchi T, Imanishi Y *et al.* Impaired myocardium regeneration with skeletal cell sheets—a preclinical trial for tissue-engineered regeneration therapy. *Transplantation* 2010;**90**:364–372.
29. Pereira RO, Carvalho SN, Stumbo AC, Rodrigues CA, Porto LC, Moura AS *et al.* Osteopontin expression in coculture of differentiating rat fetal skeletal fibroblasts and myoblasts. *In Vitro Cell Dev Biol Anim* 2006;**42**:4–7.
30. Dobaczewski M, Bujak M, Li N, Gonzalez-Quesada C, Mendoza LH, Wang XF *et al.* Smad3 signaling critically regulates fibroblast phenotype and function in healing myocardial infarction. *Circ Res* 2010;**107**:418–428.
31. Lenga Y, Koh A, Perera AS, McCulloch CA, Sodek J, Zohar R. Osteopontin expression is required for myofibroblast differentiation. *Circ Res* 2008;**102**:319–327.
32. Orlova VV, Liu Z, Goumans MJ, ten Dijke P. Controlling angiogenesis by two unique TGF-β type I receptor signaling pathways. *Histol Histopathol* 2011;**26**:1219–1230.

OPEN ACCESS Freely available online

PLOS ONE

Tightly Regulated and Homogeneous Transgene Expression in Human Adipose-Derived Mesenchymal Stem Cells by Lentivirus with Tet-Off System

Hiroyuki Moriyama[1*☯], Mariko Moriyama[1,2☯], Kei Sawaragi[1], Hanayuki Okura[2], Akihiro Ichinose[3], Akifumi Matsuyama[2], Takao Hayakawa[1]

1 Pharmaceutical Research and Technology Institute, Kinki University, Higashi-Osaka, Osaka, Japan, **2** Platform for Realization of Regenerative Medicine, Foundation for Biomedical Research and Innovation, Chuo-ku, Kobe, Hyogo, Japan, **3** Department of Plastic Surgery, Kobe University Hospital, Chuo-ku, Kobe, Hyogo, Japan

Abstract

Genetic modification of human adipose tissue–derived multilineage progenitor cells (hADMPCs) is highly valuable for their exploitation in therapeutic applications. Here, we have developed a novel single tet-off lentiviral vector platform. This vector combines (1) a modified tetracycline (tet)-response element composite promoter, (2) a multi-cistronic strategy to express an improved version of the tet-controlled transactivator and the blasticidin resistance gene under the control of a ubiquitous promoter, and (3) acceptor sites for easy recombination cloning of the gene of interest. In the present study, we used the cytomegalovirus (CMV) or the elongation factor 1 α (EF-1α) promoter as the ubiquitous promoter, and EGFP was introduced as the gene of interest. hADMPCs transduced with a lentiviral vector carrying either the CMV promoter or the EF-1α promoter were effectively selected by blasticidin without affecting their stem cell properties, and EGFP expression was strictly regulated by doxycycline (Dox) treatment in these cells. However, the single tet-off lentiviral vector carrying the EF-1α promoter provided more homogenous expression of EGFP in hADMPCs. Intriguingly, differentiated cells from these Dox-responsive cell lines constitutively expressed EGFP only in the absence of Dox. This single tet-off lentiviral vector thus provides an important tool for applied research on hADMPCs.

Citation: Moriyama H, Moriyama M, Sawaragi K, Okura H, Ichinose A, et al. (2013) Tightly Regulated and Homogeneous Transgene Expression in Human Adipose-Derived Mesenchymal Stem Cells by Lentivirus with Tet-Off System. PLoS ONE 8(6): e66274. doi:10.1371/journal.pone.0066274

Editor: Niels Olsen Saraiva Câmara, Universidade de Sao Paulo, Brazil

Received December 20, 2012; **Accepted** May 2, 2013; **Published** June 12, 2013

Funding: This work was supported in part by MEXT KAKENHI Grant Number 23791304 to M.M. and 24791927 to H.M. This work was also supported in part by grants from the Ministry of Health, Labor, and Welfare of Japan and a grant from the Program for Promotion of Fundamental Studies in Health Sciences of the National Institute of Biomedical Innovation (NIBIO). The funders had no role in study design, data collection and analysis, decision to publish, or preparation of the manuscript.

Competing Interests: The authors have declared that no competing interests exist.

* E-mail: moriyama@phar.kindai.ac.jp

☯ These authors contributed equally to this work.

Introduction

Human adipose tissue–derived mesenchymal stem cells (MSCs), also referred to as human adipose tissue–derived multilineage progenitor cells (hADMPCs), are multipotent stem cells that can differentiate into various types of cells, including hepatocytes [1], cardiomyoblasts [2], pancreatic cells [3], and neuronal cells [4–6]. They can be easily and safely obtained from lipoaspirates without posing serious ethical issues and can also be expanded ex vivo under appropriate culture conditions. Moreover, MSCs, including hADMPCs, have the ability to migrate to injured areas and secrete a wide variety of cytokines and growth factors necessary for tissue regeneration [7–11]. Because of their hypoimmunogenicity and immune modulatory effects, hADMPCs are good candidates for gene delivery vehicles for therapeutic purposes [12]. Thus, hADMPCs are an attractive material for cell therapy and tissue engineering, making the development of technologies for permanent and highly controlled genetic modification of hADMPCs quite valuable.

Lentiviral vectors are powerful tools for gene transfer in primary human cells, as they integrate into the host cell genome, resulting in stable long-term transgene expression. Lentiviral vectors are less prone to transcriptional silencing than oncoretroviral vectors [13,14]; however, researchers have reported that transgene silencing occurs when a strong promoter, such as the cytomegalovirus (CMV) promoter, is used in certain cell types, especially embryonic stem cells [15–17]. Recently, it has been reported that the CMV promoter is also silenced in rat bone marrow–derived MSCs [18,19], suggesting that consideration of promoter used in the lentiviral vector is one of the most critical issues.

In addition to the choice of promoters, the specific gene expression system can have a great impact on the properties and functions of the infected hADMPCs. In order to express therapeutic genes, master regulatory genes, or microRNAs, the development of a tightly regulated, inducible gene expression system is required. The tetracycline (tet)-regulated transgene expression (tet-off) system is the most advanced system being used in gene therapy trials [20]. Two expression cassettes need to be delivered for use of the tet-off system: the regulatory unit for the constitutive expression of the transactivator (tTA), and the tet-controlled responsive unit for the expression of the gene of interest. Traditionally, these 2 cassettes should be transduced separately to establish tet-inducible cell lines. This time-consuming process

significantly limits the number of cell lines that can be generated for target gene expression. Recently, several researchers attempted to develop single-vector–based tet-inducible lentiviral systems [21–24]. However, the large plasmid size and lack of antibiotic selectable markers in these systems made the generation of plasmid constructs, high titer lentiviral particles, and stably expressing transgenic cell lines difficult.

To overcome the limitations of the current single vector-based tet-inducible lentiviral systems, we generated a robust system that incorporates all the necessary components for tet-off gene expression, restriction enzyme treatment/ligation independent cloning system, and antibiotic selectable markers in a single lentiviral vector. This vector consists of a modified tet-response element composite promoter (TRE-Tight) followed by a Gateway cassette containing *att*R recombination sites flanking a *ccd*B gene and a chloramphenicol resistant gene, which allows for easy and rapid shuttling of the gene of interest into the vector. This vector also carries an improved version of the tet-controlled transactivator (tTA-advanced) and the blasticidin resistance gene, linked by the self-cleaving viral T2A peptide, under a ubiquitous promoter. In the present study, we examined 2 ubiquitous promoters commonly used in mammalian systems: the CMV promoter and the human polypeptide chain elongation factor 1 α (EF-1α) promoter, to determine which promoter is more efficient in hADMPCs. In addition, we also confirmed whether genetically modified hADMPCs maintained their stem cell properties following transduction with this single tet-off lentiviral vector. We examined the expression pattern of cell surface markers, as well as the cells' differentiation potential into adipocytes, chondrocytes, osteocytes, and neuronal cells. Our data demonstrated that hADMPCs transduced with our all-in-one lentiviral vector were effectively selected by blasticidin without affecting their stem cell properties, and transgene expression was strictly regulated by doxycycline (Dox) not only in undifferentiated cells but also in differentiated cells. A single tet-off lentiviral vector system thus provides a powerful tool for applied research on hADMPCs.

Materials and Methods

Adipose Tissue Samples

Subcutaneous adipose tissue samples (10–50 g each) were resected during plastic surgery in 5 women (age, 20–60 years) as excess discards. The study protocol was approved by the Review Board for Human Research of Kobe University Graduate School of Medicine, Foundation for Biomedical Research and Innovation, and Kinki University Pharmaceutical Research and Technology Institute (reference number: 10-005). Each subject provided signed informed consent.

Cell Culture

hADMPCs were isolated as previously reported [1,11,25,26] and maintained in a medium containing 60% DMEM-low glucose, 40% MCDB-201 medium (Sigma Aldrich, St. Louis, MO, USA), 1× insulin-transferrin-selenium (Life technologies, Carlsbad, CA, USA), 1 nM dexamethasone (Sigma Aldrich, St. Louis, MO, USA), 100 mM ascorbic acid 2-phosphate (Wako, Osaka, Japan), 10 ng/mL epidermal growth factor (PeproTech, Rocky Hill, NJ, USA), and 5% fetal bovine serum. The cells were plated to a density of 5×10^3 cells/cm^2 on fibronectin-coated dishes, and the medium was replaced every 2 days.

Plasmid Construction and Lentivirus Production

EGFP was cloned into a pENTR11 vector (Invitrogen) to create an entry vector, pENTR11-EGFP. To generate pTRE-RfA, the tet-responsive element (TRE) of the pTRE-Tight vector (Clontech, Mountain Veiw, CA, USA) and the Reading frame A (RfA), a Gateway cassette containing *att*R recombination sites flanking a *ccd*B gene and a chloramphenicol-resistance gene (Invitrogen) were introduced into *Xba*I-*Xho*I sites of pSico (Addgene plasmid 11578). An improved version of the tet-controlled transactivator (tTA-advanced: pTet-off-advanced Clontech) was linked to the blasticidin resistance (Bsd) gene by the viral T2A peptide to generate tTA-2A-Bsd. Briefly, 2A-Bsd was amplified by PCR using the following primers:

2A-Bsd F: GGGGGATCCGGCGAGGGCAGAGGAAGTCTTCTAACATGCGGTGACGTGGAGGAAAATCCCGGGCCCATGAAGACCTTCAACATCTCTCAG, Bsd R: GCGAGATCTTTAGTTCCTGGTGTACTTG. The resultant product was confirmed by sequencing and ligation with the SmaI site of tTA. EF promoter/CMV promoter and tTA-2A-Bsd was introduced into pTRE-RfA to produce pTRE-RfA-EF-tTA-2A-Bsd or pTRE-RfA-CMV-tTA-2A-Bsd. The entry vector pENTR11-EGFP and pTRE-RfA-EF-tTA-2A-Bsd, pTRE-RfA-CMV-tTA-2A-Bsd, CSII-EF-RfA, or CSII-CMV-RfA (kindly provided by Dr. Miyoshi, RIKEN BioResource Center, Tsukuba, Japan) were incubated with LR clonase II enzyme mix (Invitrogen) to generate pTRE-EGFP-EF-tTA-2A-Bsd, pTRE-EGFP-CMV-tTA-2A-Bsd, CSII-EF-EGFP or CSII-CMV-EGFP. The resultant plasmid was mixed with packaging plasmids (pCAG-HIVg/p and pCMV-VSVG-RSV-Rev, kindly provided by Dr. Miyoshi) and transfected into 293T cells. The supernatant medium, which contained lentiviral vectors, was collected 2 days after transduction and concentrated by centrifugation (6000× *g*, 15 h, 4°C). Viral titers (transduction unit: TU) were determined by serial dilution on 293T cells and the percentage of EGFP positive cells was measured by Guava easyCyte 8HT flow cytometer (Merck-Millipore, Billerica, MA, USA).

Plasmid Propagation in *E. coli*

DH5α (F-, Φ80dlacZΔM15, Δ(lacZYA-argF)U169, deoR, recA1, endA1, hsdR17(rK-, mK+), phoA, supE44, λ-, thi-1, gyrA96, relA1) were used for general purpose. To propagate plasmids containing the ccdB gene, One Shot® ccdB Survival™ 2 T1 Phage-Resistant (T1R) chemically competent *E. coli* (Invitrogen) were used.

Western Blot Analysis

Cells were washed with ice-cold phosphate-buffered saline and lysed with M-PER Mammalian Protein Extraction Reagent (Thermo Scientific Pierce, Rockford, IL, USA). Equal amounts of proteins were separated by sodium dodecyl sulfate polyacrylamide gel electrophoresis, transferred to polyvinylidene fluoride membranes (Immobilon-P; Merck-Millipore), and probed with antibody against TetR (from Clontech). Horseradish peroxidase (HRP)-conjugated anti-mouse secondary antibody (Cell Signaling Technology, Danvers, MA, USA) was used as a probe, and immunoreactive bands were visualized with the Immobilon Western Chemiluminescent HRP substrate (Millipore). The band intensity was measured using ImageJ software.

Flow Cytometry Analysis

hADMPCs were seeded at a density of 2×10^4 cells per well in 12-well culture plates and were transduced with CSII-EF-EGFP or CSII-CMV-EGFP at a multiplicity of infection (m.o.i.) of 25, 50,

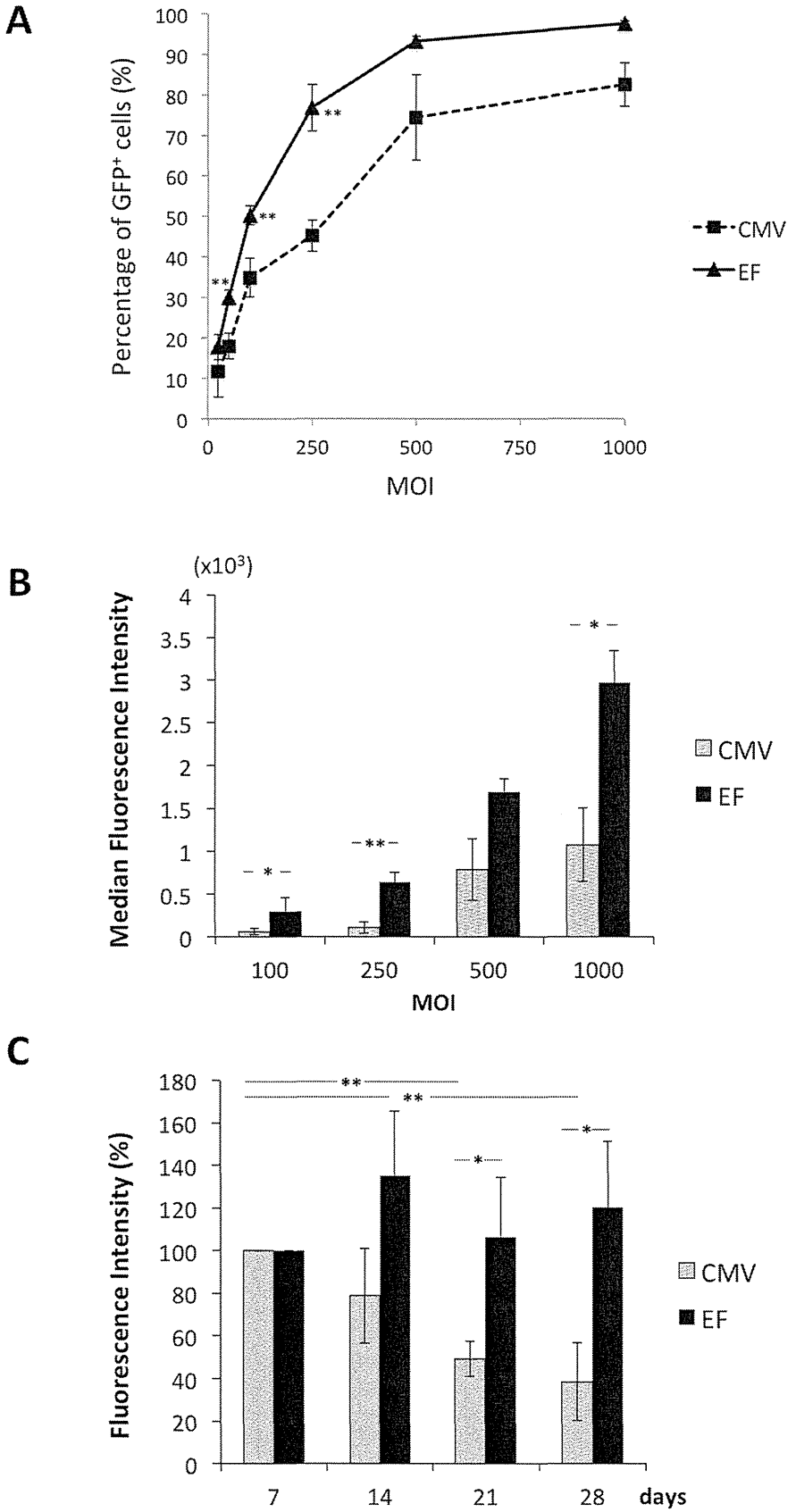

Figure 1. The efficiency of CMV or EF-1α promoter in hADMPCs. Lentiviral vectors encoding EGFP under the control of CMV or EF-1α promoter were transduced with hADMPCs at m.o.i. of 25, 50, 100, 250, 500, and 1000, and the cells were analyzed by flow cytometry. (A) The percentage of EGFP-positive hADMPCs transduced with CSII-CMV-EGFP (CMV) or CSII-EF-EGFP (EF). (B) (C) The median fluorescence intensities of the

EGFP-expressing populations. (B) hADMPCs transduced with CSII-CMV-EGFP or CSII-EF-EGFP at m.o.i. of 100, 250, 500, and 1000 were analyzed. (C) hADMPCs transduced with CSII-CMV-EGFP or CSII-EF-EGFP at m.o.i. of 1000 were analyzed over a 28 day period. Error bars represent the standard error of 3 independent analyses. **, $P<0.01$; *, $P<0.05$ (Student's t test).
doi:10.1371/journal.pone.0066274.g001

100, 250, 500, and 1000. Four days later, the cells were analyzed with a Guava easyCyte 8HT flow cytometer (Merck-Millipore) using an argon laser at 488 nm. Dead cells were excluded with the LIVE/DEAD fixable far red dead cell stain kit (Invitrogen). For analysis of hADMPCs transduced with pTRE-EGFP-EF-tTA-2A-Bsd or pTRE-EGFP-CMV-tTA-2A-Bsd, hADMPCs were transduced with the lentiviral vector at a m.o.i. of 250 and were cultured with or without 1 μg/mL Dox. Four days later, a part of the cells were analyzed with a Guava easyCyte 8HT flow cytometer. The rest of the cells were cultured with 4 μg/mL blasticidin and 1 μg/mL Dox for 3 weeks. Then, the cells were seeded in 6-well plates and cultured with or without Dox for 4 days. The cells were harvested and re-suspended in staining buffer (PBS containing 1% BSA, 2 mM EDTA, and 0.01% sodium azide) at a density of 1×10^6 cells/mL and incubated with phycoerythrin (PE)-conjugated antibody against CD13, CD29, CD34, CD44, CD73, CD90, CD105, or CD166 for 20 min. Non-specific staining was assessed using relevant isotype controls. 525/30 nm and 583/26 nm band pass filters were used for the detection of EGFP and PE, respectively. Dead cells were excluded with the LIVE/DEAD fixable far red dead cell stain kit (Invitrogen). FlowJo software (TreeStar Inc., Ashland, OR, USA) was used for quantitation analysis. The threshold for gating was determined as the fluorescence value above which less than 1% of the control cells were considered as positive events.

Fluorescence Microscopy

Phase contrast and fluorescence images were obtained using Fluorescence Microscope (BZ-9000; Keyence, Osaka, Japan) using BZ Analyzer Software (Keyence).

Adipogenic, Osteogenic, Chondrogenic, and Neurogenic Differentiation Procedures

For adipogenic differentiation, cells were cultured in differentiation medium (Zen-Bio, Durham, NC, USA). After 3 days, half of the medium was changed to adipocyte medium (Zen-Bio), and this was repeated every 3 days. Three weeks after differentiation, characterization of adipocytes was confirmed by microscopic observation of intracellular lipid droplets by oil red O staining. Osteogenic differentiation was induced by culturing the cells in DMEM containing 10 nM dexamethasone, 50 mg/dL ascorbic acid 2-phosphate, 10 mM β-glycerophosphate (Sigma), and 10% FBS. Differentiation was examined by alizarin red staining. For chondrogenic differentiation, 2×10^5 hADMPCs were centrifuged at $400\times$ *g* for 10 min. The resulting pellets were cultured in chondrogenic medium (α-MEM supplemented with 10 ng/mL transforming growth factor-β, 10 nM dexamethasone, 100 mM ascorbate, and 1× insulin–transferrin–selenium solution) for 14 days, as described previously [27]. The pellets were fixed with 4% paraformaldehyde in PBS, embedded in OCT, frozen, and sectioned at 8 μm. The sections were incubated with PBSMT (PBS containing 0.1% Triton X-100, 2% skim milk) for 1 h at room temperature, and then incubated with mouse monoclonal antibody against type II collagen (Abcam, Cambridge, MA, USA) and rabbit polyclonal antibody against GFP (Invitrogen) for 1 h. After washing with PBS, cells were incubated with Alexa 546 conjugated anti-mouse IgG and Alexa 488 conjugated anti-rabbit IgG for chondrocytes (Invitrogen) or Alexa 546 conjugated anti-rabbit IgG and Alexa 488 conjugated anti-rat IgG (Invitrogen) for neuronal cells. The cells were counterstained with 4′-6-diamidino-2-phenylindole (DAPI) (Invitrogen) to identify cellular nuclei. For neurogenic differentiation, cells were cultured in Hyclone AdvanceSTEM neural differentiation medium (Thermo Scientific, South Logan, UT, USA) for 2 days. Differentiation was examined by immunofluorescent staining against β3-tubulin. Cells were fixed with 4% paraformaldehyde in PBS for 10 min at 4°C and then washed 3 times in PBS. Blocking was performed with PBSMT for 1 h at room temperature. The differentiated cells were incubated with rabbit monoclonal antibody against β3-tubulin (Cell Signaling Technologies, Danvers, MA, USA) and rat monoclonal antibody against GFP (Nacalai, Kyoto, Japan). After washing with PBS, cells were incubated with Alexa 546 conjugated anti-rabbit IgG and Alexa 488 conjugated anti-rat IgG (Invitrogen). The cells were counterstained with 4′-6-diamidino-2-phenylindole (DAPI) (Invitrogen) to identify cellular nuclei.

Results

The Efficiency of the EF-1α Promoter was Higher than that of the CMV Promoter in hADMPCs

To determine the efficiency of the EF-1α promoter and the CMV promoter, hADMPCs were transduced with CSII-EF-EGFP or CSII-CMV-EGFP at a m.o.i. of 25, 50, 100, 250, 500, and 1000 and analyzed by flow cytometry. As shown in Figure 1A, percentage of GFP-positive cells increased in a dose-dependent manner. Intriguingly, transduction efficiency of CSII-EF-EGFP was significantly higher than that of CSII-CMV-EGFP in hADMPCs (Figure 1A). Moreover, a higher induction level of GFP was observed under the EF-1α promoter than under the CMV promoter, based on the median fluorescent intensity (Figure 1B). Furthermore, GFP fluorescent intensities driven from the CMV promoter were significantly decreased (from 100% on day 7 to 49.3% on day 21 and 38.4% on day 28; Figure 1C), indicating that promoter silencing occurred as previously reported [19]. In contrast, hADMPCs transduced with CSII-EF-EGFP sustained GFP expression levels with no significant reduction throughout the 28-day experimental period (Figure 1C).

Construction and Characterization of Dual-promoter Lentiviral Vectors in hADMPCs

Next, we constructed dual-promoter lentiviral vectors, which contain TRE-Tight followed by an improved version of tet-controlled transactivator (tTA advanced) induced under the CMV or EF-1α promoter (Figure 2A). In this "single tet-off lentiviral vector platform", the regulator and response elements are combined in a single lentiviral genome, along with a Gateway cassette containing *att*R recombination sites flanking a *ccd*B gene and a chloramphenicol-resistance gene, which allows an easy and rapid shuttling of the gene of interest into the vectors using the Gateway LR recombination reaction (Figure 2A). Using this system, we constructed pTRE-EGFP-CMV-tTA-2A-Bsd or pTRE-EGFP-EF-tTA-2A-Bsd (Figure 2B). Both the CMV and the EF-1α promoters drive the mRNA expression of tTA advanced linked to the Bsd gene by the Thosea asigna virus 2A (T2A) peptide sequence. This single transcript is then translated and cleaved into 2 proteins; tTA advanced carrying 2A tag at the

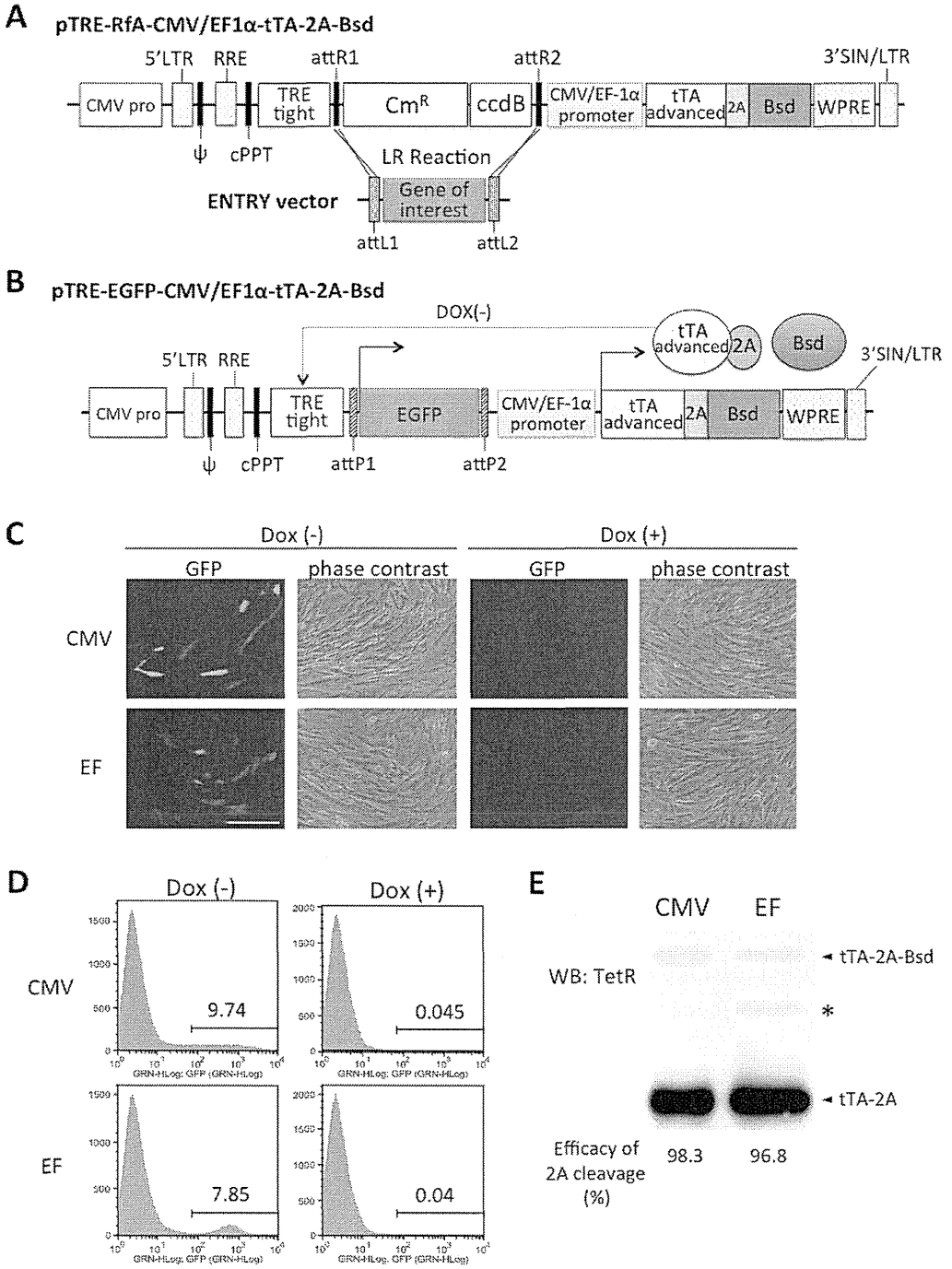

Figure 2. Schematic drawings of the single lentiviral vectors for tet-off system used in this work. (A) Gateway-compatible destination vectors containing *att*R recombination sites flanking a *ccd*B gene and a chloramphenicol-resistance gene, which allows an easy and rapid shuttling of gene of interest flanked by attL sites into the destination vectors using the Gateway LR recombination reaction. They also have an improved version of tetracycline-controlled transactivator (tTA) linked to the blasticidin resistant (Bsd) gene by the Thosea asigna virus 2A (2A) peptide sequence, whose expression is regulated by the CMV or EF-1α promoter. In the present study, we constructed an entry vector encoding EGFP flanked by attL, resulting in a destination clone, pTRE-EGFP-CMV-tTA-2A-Bsd or pTRE-EGFP-EF-tTA-2A-Bsd (B). In the absence of doxycycline (Dox), tTA-2A binds to the TRE-Tight promoter and activates EGFP transcription. For more details, see the Results section. CMV pro, CMV promoter; LTR, long terminal repeats; ψ, packaging signal; RRE, rev response elements; cPPT, central polypurine tract; TRE, tet-responsive element; Cm^R, chloramphenicol resistance; tTA, tetracycline-controlled transactivator; Bsd, blasticidin resistance; WPRE, woodchuck hepatitis virus posttranscriptional control element; SIN, self-inactivating. (C) (D) hADMPCs were transduced with pTRE-EGFP-CMV-tTA-2A-Bsd or pTRE-EGFP-EF-tTA-2A-Bsd at m.o.i. of 250. Four days after transduction, the cells were divided into 2 populations; with 1 μg/mL of Dox (Dox (+)) and without Dox (Dox (-)). (C) Fluorescent and phase contrast images. Scale bar, 200 μm. (D) Log fluorescence histograms of EGFP by flow cytometry analysis. (E) The whole cell lysates from hADMPCs transduced with pTRE-EGFP-CMV-tTA-2A-Bsd or pTRE-EGFP-EF-tTA-2A-Bsd were subjected to western blotting to monitor the cleavage efficiency of tTA-2A-Bsd proteins. A primary antibody against TetR was used to detect either tTA-2A-Bsd (non-cleaved form) or tTA-2A (cleaved form). Asterisk indicates a nonspecific band.

doi:10.1371/journal.pone.0066274.g002

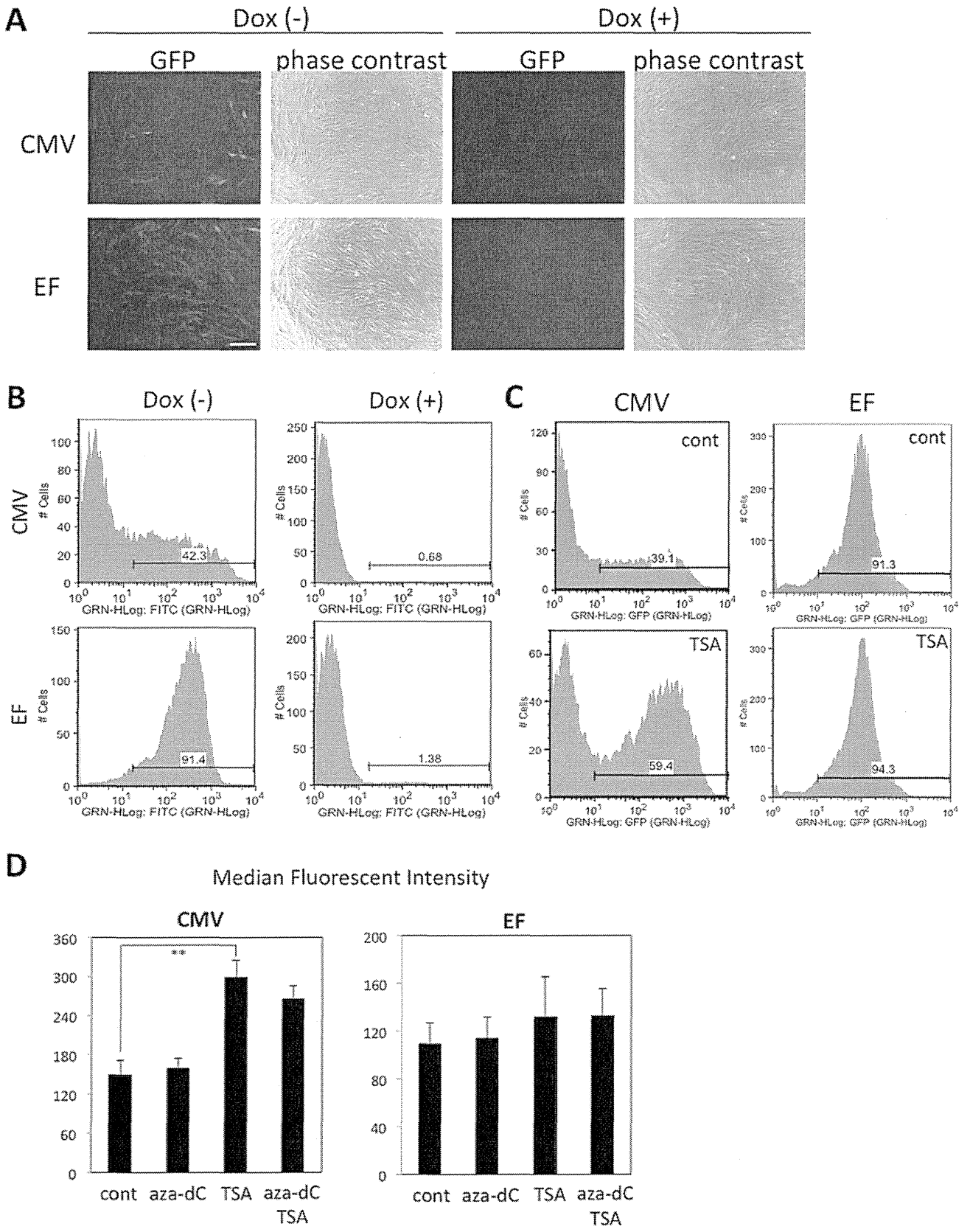

Figure 3. Blasticidin selection of hADMPCs transduced with single tet-off lentiviral vector platform. hADMPCs were transduced with pTRE-EGFP-CMV-tTA-2A-Bsd (CMV) or pTRE-EGFP-EF-tTA-2A-Bsd (EF) at m.o.i. of 250. The cells were treated with 4 μg/mL blasticidin and 1 μg/mL Dox for 2 weeks. Then, the cells were cultured in the absence (Dox (-)) or presence (Dox (+)) of 1 μg/mL Dox for 4 days, and analyzed under a microscope (A) and flow cytometer (B). The cells were treated with 100 nM TSA (TSA), 5 μM 5-aza-dC (aza-dC), or both for 48 h before analyzed by flow

cytometer. (C) A representative fluorescence histogram of EGFP. (D) The median fluorescence intensities of the EGFP-expressing populations. Error bars represent the standard error of 3 independent analyses. **, P<0.01 (Student's t test). Scale bar, 200 μm.
doi:10.1371/journal.pone.0066274.g003

C-terminus (tTA-2A) and Bsd. tTA-2A binds to the TRE-tight in the absence of Dox, a tet derivative, and activates transcription of EGFP to a very high level. In the presence of Dox, tTA-2A is unable to bind the TRE-Tight in a tet-responsive promoter, and the system is inactive.

To investigate the usefulness of these lentiviral vectors, hADMPCs were transduced with pTRE-EGFP-CMV-tTA-2A-Bsd or pTRE-EGFP-EF-tTA-2A-Bsd at a m.o.i. of 250. As shown in Figure 2C, expression of EGFP was observed in the absence of Dox, whereas addition of Dox (1 μg/mL) was enough to suppress the expression. Flow cytometry analysis revealed that the transduction efficiency was relatively low (EGFP-positive cells were 7.5~10%) compared with that of CSII-CMV-EGFP or CSII-EF-EGFP (EGFP-positive cells were 45% or 77% at a m.o.i. of 250, respectively; Figure 1A), and the tet-off system completely abolished gene expression in the presence of Dox (Figure 2D). Flow cytometry analysis also revealed that fluorescent intensity was relatively uniform in hADMPCs transduced with pTRE-EGFP-EF-tTA-2A-Bsd, but a wide range of fluorescent intensities was observed in hADMPCs infected with pTRE-EGFP-CMV-tTA-2A-Bsd. These data suggest that tTA-2A functions properly in this system. Moreover, western blot analysis against tTA showed the efficient cleavage (>95%) of tTA-2A-Bsd proteins into tTA-2A and Bsd (Figure 2E).

To further determine that Bsd cleaved from tTA-2A-Bsd was effective in this system, 4 μg/mL blasticidin was administered to hADMPCs. Within 1 week after the selection, control hADMPCs were completely killed (data not shown), whereas hADMPCs that were successfully transduced with either pTRE-EGFP-CMV-tTA-2A-Bsd or pTRE-EGFP-EF-tTA-2A-Bsd could survive and proliferate, demonstrating that Bsd from tTA-2A-Bsd is sufficient to confer blasticidin resistance to the cells. The surviving cells were kept in culture medium with blasticidin and then divided into 2 populations, either with Dox (1 μg/mL) or without Dox. As shown in Figure 3A and 3B, almost all (>90%) the cells transduced with pTRE-EGFP-EF-tTA-2A-Bsd strongly expressed EGFP in the absence of Dox. In hADMPCs transduced with pTRE-EGFP-CMV-tTA-2A-Bsd, however, >50% of the cells were EGFP negative regardless of their blasticidin resistance. Moreover, fluorescent intensities were quite variable; some cells expressed very high levels of EGFP, while others expressed very low levels (Figure 3A and 3B). This might be due to "promoter suppression," transcript repression of an upstream transcriptional unit by a downstream unit when 2 transcriptional units lie adjacent in head-to-tail tandem on a chromosome [28,29]. Studies have revealed that the suppression by adjacent units is epigenetic and involves modification of the chromatin structure, including DNA methylation at CpG sites within the promoter, histone deacetylation, histone methylation at specific residues (e.g., H3K9, H3K27), and densely packed nucleosomes that create a closed chromatin structure. In order to determine if inhibiting histone deacetylases or DNA methylation would re-induce EGFP expression, pTRE-EGFP-CMV-tTA-2A-Bsd cells were treated with histone deacetylase inhibitor trichostatin A (TSA) and/or DNA methylation inhibitor 5-aza-2′-deoxycytidine (5-aza-dC). TSA treatment significantly increased the number of EGFP-positive cells and strengthened the fluorescent intensities of EGFP, whereas 5-aza-dC had no effect, suggesting that EGFP expression was repressed by histone deacetylation when stably transduced with pTRE-EGFP-CMV-tTA-2A-Bsd (Figure 3C and 3D). These inhibitors had no effect on hADMPCs transduced with pTRE-EGFP-EF-tTA-2A-Bsd. These data suggest that the dual-promoter lentiviral vector using the EF promoter is more resistant to gene silencing than that using the CMV promoter.

Blasticidin-selected hADMPCs Maintain the Properties of Their Parental hADMPCs

hADMPCs are an attractive material for cell therapy because of their ability to secrete various cytokines and growth factors. These cells also have the ability to differentiate into various types of cells, including adipocytes, chondrocytes, osteocytes, hepatocytes, cardiomyoblasts, and neuronal cells. Gene manipulation of hADMPCs may thus generate great possibilities for cell therapy and tissue engineering. From this point of view, the development of an efficient and stable Dox-responsive gene transfer system to achieve high levels of transgene expression in hADMPCs, without affecting the phenotype, is of special interest for the field. We therefore studied the cell properties of hADMPCs transduced with the single tet-off lentiviral vector after blasticidin selection. Flow cytometry analysis revealed no changes in the expression of the main surface markers (positive for CD13, CD29, CD44, CD73, CD90, CD105, and CD166, and negative for CD34) either in the absence or presence of Dox (Figure 4). To further confirm the properties of hADMPCs, the cells were differentiated into adipocytes, osteocytes, chondrocytes, and neuronal cells. As shown in Figure 5, blasticidin-selected hADMPCs maintained their ability to differentiate into adipocytes, osteocytes, chondrocytes, and neuronal cells. Moreover, EGFP was stably expressed in the differentiated cells only in the absence of Dox (Figure 5).

Discussion

In recent years, there is growing interest in the use of MSCs for cell therapy and tissue engineering because of their differentiation potential and ability to secrete growth factors [7–11]. Furthermore, because of their hypo-immunogenicity and immune modulatory effects, MSCs are good candidates for gene delivery vehicles for therapeutic purposes [12,14]. In addition to primary MSCs, genetically modified MSCs have been applied to bone regeneration, muscle repair, diabetes, Parkinson's disease, and myocardial infarction recovery [14,30–35]. Duan et al. reported that the angiogenic effect of MSCs could be enhanced by adenovirus-mediated HGF overexpression in the treatment of cardiac ischemia injury [14]. Karnieli et al. and Li et al. both reported the reversal of hyperglycemia in streptozotocin-induced diabetic mice after transplantation of insulin-producing cells originating from genetically modified Pdx-1 expressing MSCs [32,33].

While significant progress has been made in the use of genetically modified MSCs for basic and applied research, the current methods for gene manipulation are still insufficient for some applications. Adenoviral vectors are commonly used for transient expression because they remain epichromosomal in the host cells, and their ability to transiently infect target cells minimizes the risk of insertional mutagenesis [36]. However, relatively brief transgene expression may limit the utility of this approach to tissue repair applications. On the other hand, lentiviral vectors, which are promising vectors for gene delivery in primary human cells, integrate into the host cell genome, which may be an appropriate strategy for tissue repair applications

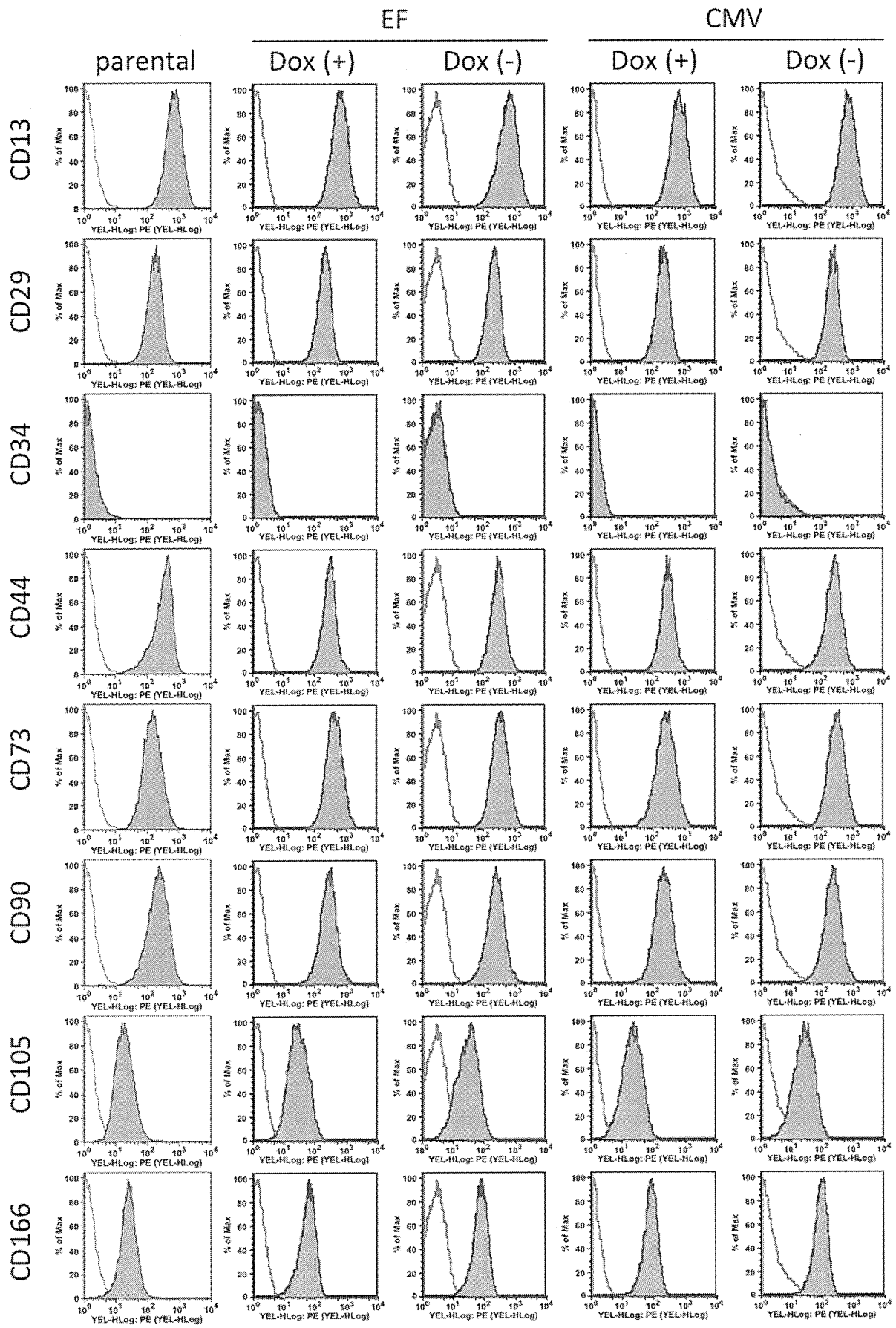
EF
CMV
parental
Dox (+)
Dox (-)
Dox (+)
Dox (-)
CD13
CD29
CD34
CD44
CD73
CD90
CD105
CD166
% of Max
YEL-HLog: PE (YEL-HLog)

Figure 4. Expression pattern of surface cell markers on Dox-responsive hADMPCs. Dox-responsive hADMPCs after selection by blasticidin were cultured in the absence (Dox(-)) or presence (Dox (+)) of 1 μg/mL Dox for 4 days. Expression of the different surface markers were analyzed by flow cytometry and compared to the expression by a parental hADMPCs. They were stained with PE-coupled antibodies against CD13, CD29, CD34, CD44, CD73, CD90, CD105, and CD166. Histogram of a PE-coupled mouse IgG1 κ isotype control is shown in gray. CMV; hADMPCs transduced with pTRE-EGFP-CMV-tTA-2A-Bsd, EF; hADMPCs transduced with pTRE-EGFP-EF-tTA-2A-Bsd.
doi:10.1371/journal.pone.0066274.g004

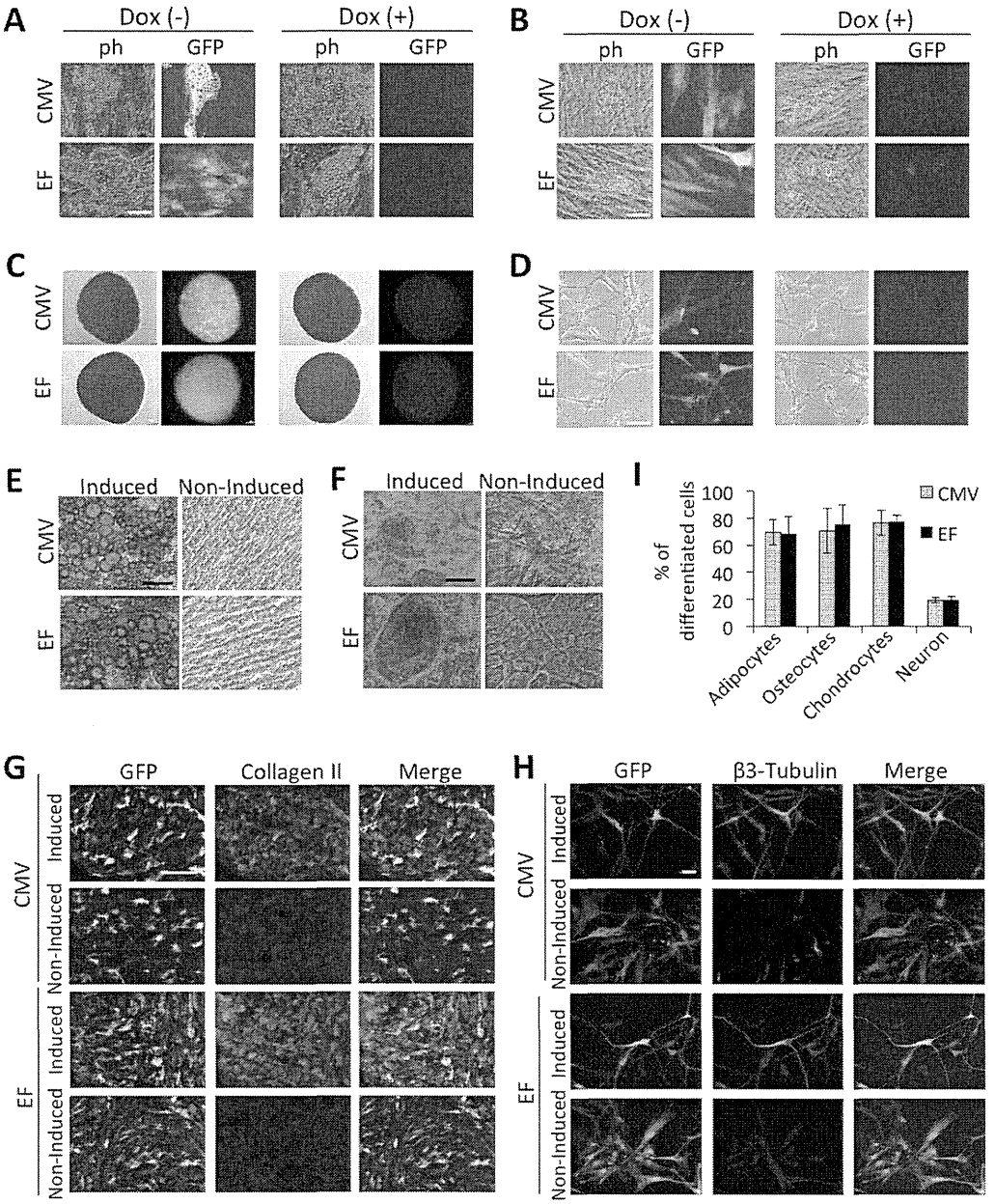

Figure 5. Differentiation potential of Dox-responsive hADMPCs. Dox-responsive hADMPCs were differentiated into adipocytes (A, E), osteocytes (B, F), chondrocytes (C, G), and neuronal cells (D, H). (A–D) Phase contrast (ph) and fluorescent (GFP) images. Dox-responsive hADMPCs were differentiated in the absence of Dox (Dox(−)) or in the presence of 1 μg/mL Dox (Dox(+)) as described in the material and methods section. (E–I) Confirmation of differentiated cells by oil red O staining for adipocytes (E), alizarin red staining for osteocytes (F), immunohistochemical staining against collagen II for chondrocytes (G), and immunohistochemical staining against β3-tubulin for neuronal cells (H). The percentages of differentiated cells to each cell type were calculated by the computerized image analysis (I). Cells that were not induced to differentiate (non-induced) were used as a negative control. CMV; hADMPCs transduced with pTRE-EGFP-CMV-tTA-2A-Bsd, EF; hADMPCs transduced with pTRE-EGFP-EF-tTA-2A-Bsd. Scale bar, 50 μm.
doi:10.1371/journal.pone.0066274.g005